Head Office: Università degli Studi di Padova

Department of Biology

Ph.D. COURSE IN: BIOSCIENCES
CURRICULUM: GENETICS, GENOMICS AND BIOINFORMATICS
SERIES XXXI

THE ZEBRAFISH ORTHOLOGUE OF THE HUMAN HEPATOCEREBRAL DISEASE GENE *MPV17* PLAYS PLEIOTROPIC ROLES IN MITOCHONDRIA

Thesis written with the financial contribution of Fondazione Cariparo and Fondazione Telethon

Coordinator: Prof. Ildiko' Szabo'
Supervisor: Prof. Francesco Argenton

Ph.D. student: Laura Martorano

We are partly mitochondria;
they constitute about one-tenth of our cell volume,
one-tenth of us.
Because they are virtually the only colored part of the cell,
the mitochondria constitute the color of our tissues.
If it were not for the melanin in our skin,
myoglobin in our muscle,
and hemoglobin in our blood,
we would change color
when we exercised or ran out of breath,
so that you could tell how energized
someone was from his or her mitochondrial color."

Guy C. Brown,
The Energy of Life

To those who make my life colorful every day.

Table of contents

Abstract

Mitochondrial DNA depletion syndromes (MDS) are a group of rare autosomal recessive disorders with early onset and no cure available. MDS are caused by mutations in several nuclear genes, involved in mitochondrial DNA (mtDNA) maintenance, characterized by a strong reduction of mtDNA copy number in affected tissues and severe defects in mitochondrial functionality. Mutations in *MPV17*, a nuclear gene encoding a mitochondrial inner membrane protein, have been specifically associated with hepatocerebral forms of MDS. However, MPV17 protein function is still unclear, although it has been suggested a primary role in mtDNA maintenance. Zebrafish represents a model to clarify this biological question: a *mpv17* null mutant (*roy orbison*) shows a 19 bp deletion resulting in aberrant splicing between the exons 2 and 3 of *mpv17* gene and lacks the guanine-based reflective skin cells named iridophores. In our work, we have characterized in details the mitochondrial phenotype of *roy* larvae and found early severe ultrastructural alterations in liver mitochondria; we could also observe a significant impairment of respiratory chain complexes leading to mitochondrial quality control activation. Our results provide evidences for Mpv17 being essential in mitochondrial cristae maintenance and OXPHOS functionality, while its effect on mtDNA seems to be consequential, considering that mtDNA depletion only appear at later stages of development. Moreover, taking into account that in *roy orbison* it has been previously postulated a role for Mpv17 in purines availability, and that embryos blocked in their pyrimidine synthesis resemble *roy* phenotype, we investigated the two alternatives by administrating purine and pyrimidine precursors to homozygous mutant embryos. Interestingly, orotic acid (OA) administration ameliorated *roy* phenotype, hence linking the loss of Mpv17 to pyrimidine *de novo* synthesis. In particular, the treatment with OA, currently used as food supplement, significantly increased not only iridophores number but also the mtDNA content of *mpv17* null mutants, thus opening up a new and simple therapeutic opportunity for *MPV17*-related MDS.

Introduction

1. The mitochondrion

In the last few years, the scientific scenario identified mitochondria as key players in a growing spectrum of human diseases. These complex intracellular organelles with bacterial origin are provided with their own genome and found in the cytoplasm of almost all eukaryotic cells. Their main function concerns oxidative phosphorylation and energy metabolism. However, mitochondria are also embedded in many signaling pathways, including calcium and ROS homeostasis, as well as apoptosis. Moreover, mitochondria are known to be the major cellular ATP suppliers, via the oxidative phosphorylation (OXPHOS) system, which is composed of four enzymatic complexes, namely complexes I-IV acting in concert with the ATP synthase, and takes place inside the inner mitochondrial membrane (IMM). Mitochondrial functionality requires a synergistic relationship between mitochondrial genome (mtDNA) and nuclear genome (nDNA) (Chinnery and Hudson, 2013). The human mtDNA, a double-stranded DNA molecule of 16.6 kb, encodes only 13 subunits of the respiratory chain (RC), 2 mitochondrial ribosomal RNA (rRNA) and 22 mitochondrial transfer RNA (tRNA), while the remaining approximately 1500 mitochondrial proteins are encoded by nDNA and then imported into the organelle (Calvo *et al.*, 2016). In particular, replication and maintenance of mtDNA entirely relies on a set of nDNA-encoded proteins, underlying an essential role for the nucleus in mitochondrial biogenesis and functionality. Hence, it has been postulated that during evolution most of the genes, originally encoded by mtDNA, have been transferred to the nDNA, while others have been conceivably replaced by preexisting nuclear genes with similar function

(Gunbin *et al.*, 2017). Thus, the qualitative and quantitative maintenance of mitochondrial functionality is under the dual control of both nuclear and mitochondrial DNA and genetic alterations occurring in both genomes can affect mtDNA stability and energy production.

2. Mitochondrial DNA Depletion Syndromes

Each mitochondrion may contain hundreds of copies of mtDNA and, given that a cell is able to enclose many mitochondria, mtDNA copies per cell can be thousands. Taking into account that energy request depends on age, tissue and life style, even in physiological conditions the amount of mtDNA differs between cell types and individuals, and the relevance of this variation for cell physiology or human health has not yet been fully understood (Suomalainen and Isohanni, 2010). What has become clear, however, is that having the correct mtDNA amount in each tissue is crucial. In fact, mtDNA depletion has been discovered to cause a continuously increasing group of severe human diseases called mtDNA depletion syndromes (MDS). MDS are a clinically heterogeneous group of autosomal recessive mitochondrial disorders, first described in 1991 (Moraes *et al.,*1991), whose symptoms typically appear during infancy and childhood, with a poor prognosis and no available cure yet.

MDS are characterized by the reduction of mtDNA copy number in affected tissues and caused by the mutations of several nuclear genes involved in mtDNA replication, maintenance and stability. MDS may affect either a specific organ or a combination of organs, including muscle, liver, brain, and kidney (Fig.1).

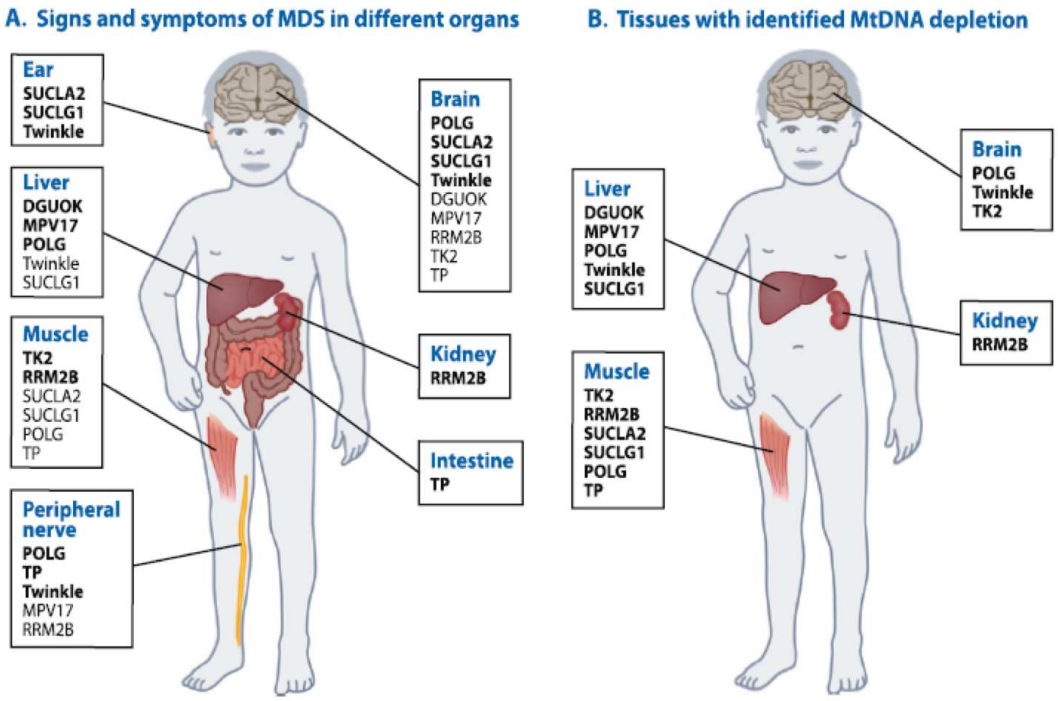

Figure 1. "MDS genes and clinical features (A). Tissues in which mtDNA depletion has been reported (B). The most common sites where depletion is detected are the liver and the skeletal muscle", from Suomalainen and Isohanni, 2010.

In these organs, mtDNA depletion results in an insufficient synthesis of RC subunits, leading to severe mitochondrial dysfunctions, including reduced respiratory efficiency and deficient energy production (Sarzi *et al.*, 2007). The tissue-specificity of MDS reflects the different sensitivity to mitochondrial malfunctions: in fact, affected organs are those that are characterized by the highest need of energy and, thus, the most damaged by the mtDNA depletion.

From a clinical point of view, these syndromes are usually classified in four different forms: i) myopathic, caused by mutations in *TK2* gene; ii) hepatocerebral, associated to mutations in *DGUOK*, *MPV17*, *POLG*, or *C10orf2*; iii) encephalomyopathic, caused by mutations occurring in *SUCLA2*, *SUCLG1*, or *RRM2B;* and iv) neurogastrointestinal, associated to *TYMP* dysfunctions (Suomalainen and Isohanni, 2010).

The phenotypical variability of MDS makes these disorders very difficult to diagnose and within each group there is a strong clinical variability. In addition, several types of MDS, caused by mutations occurring in different genes, may show overlapping symptoms (Fig.2).

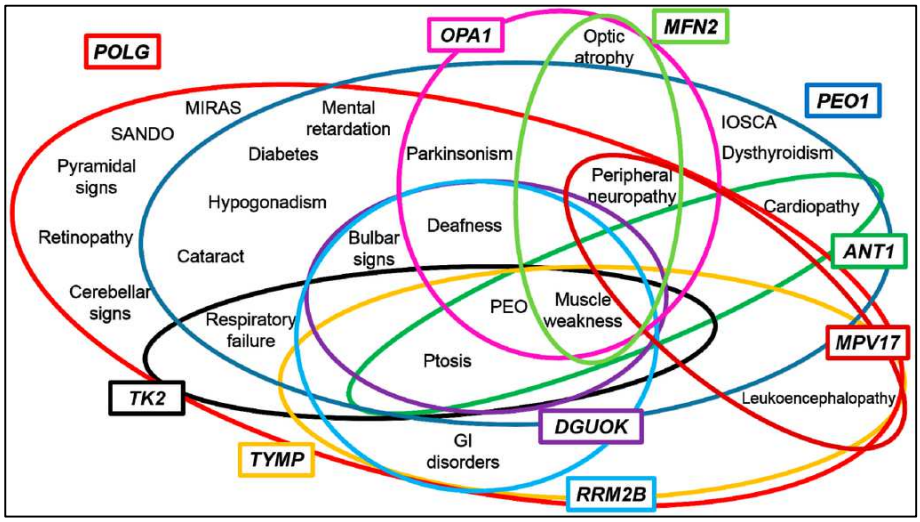

Figure 2. Nuclear genes involved in mtDNA maintenance syndromes and related clinical features (Ahmed et al., 2015).

When patients are diagnosed with MDS during their infancy, they usually show hypotonia, lactic acidosis, severe hepatopathy or renal involvement, a reduced activity of RC, and, more importantly, a low mtDNA/nDNA ratio in affected tissues. The latter molecular phenotype is indeed sufficient to confirm a clinical diagnosis of MDS.

All the MDS-causative genes which have been discovered so far are nDNA-encoded genes affecting mtDNA maintenance and stability by acting either on mtDNA replication or in the maintenance of mitochondrial deoxyribonucleotide (dNTP) pool (Fig.3).

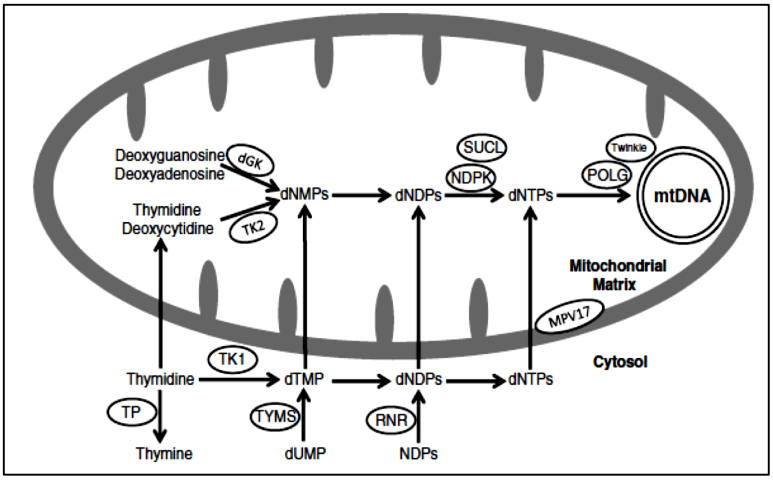

Figure 3. Schematic representation of nuclear gene-encoded proteins involved in mitochondrial nucleotide pool maintenance and mitochondrial DNA replication (El-Hattab and Scaglia, 2013).

Since mtDNA replicates independently of cell division, the mitochondrial uptake of dNTP depends either on their cytosolic synthesis via the *de novo* pathway, which is cell cycle-regulated and thus activated only in S-phase cells, or on their availability as preexisting deoxyribonucleosides, metabolized via the salvage pathway. As mtDNA synthesis is constant throughout the cell cycle, the salvage pathway is essential for mtDNA stability. *TK2*, *DGUOK*, *SUCLA2*, *SUCLG1*, *RRM2B*, and *TYMP* are mitochondrial and cytosolic enzymes taking part in nucleotide salvage pathways, hence involved in mitochondrial dNTP pool maintenance; therefore, mutations in any of these genes result in depleting mitochondria from DNA building blocks with subsequent mtDNA depletion (El-Hattab and Scaglia, 2013).

Another group of MDS-causative genes is represented by *POLG* and *C10orf*, respectively encoding the catalytic subunit of mitochondrial Polymerase and the helicase Twinkle. Both genes are essential for mtDNA replication and their mutations result in insufficient mtDNA synthesis, hence leading to mtDNA depletion.

Finally, mutation in *MPV17* gene are responsible for a hepatocerebral form of MDS. Unfortunately, although many works have been carried out in several animal and cellular models, to date the function of MPV17 remains unclear.

3. *MPV17*-related MDS

3.1 *MPV17* gene

MPV17 gene has been identified in the '90s and then included among MDS causative genes in 2006 by Spinazzola and colleagues (Spinazzola *et al.*, 2006). Human *MPV17* gene is located on chromosome 2p21-23, contains eight exons encoding 176 amino acids (aa) and is expressed in pancreas, kidney, muscle, liver, lung, placenta, brain and heart (Uusimaa *et al.*, 2014). It encodes a mitochondrial inner membrane protein with a molecular weight of 18 kDa, which shows four trans-membrane domains and both its N- and C- terminal projected to the intermembrane space (Uusimaa *et al.*, 2014). *MPV17* pathological variants have been identified all along the protein sequence, which is known to contain four cysteine residues and three putative phosphorylation sites (Fig.4).

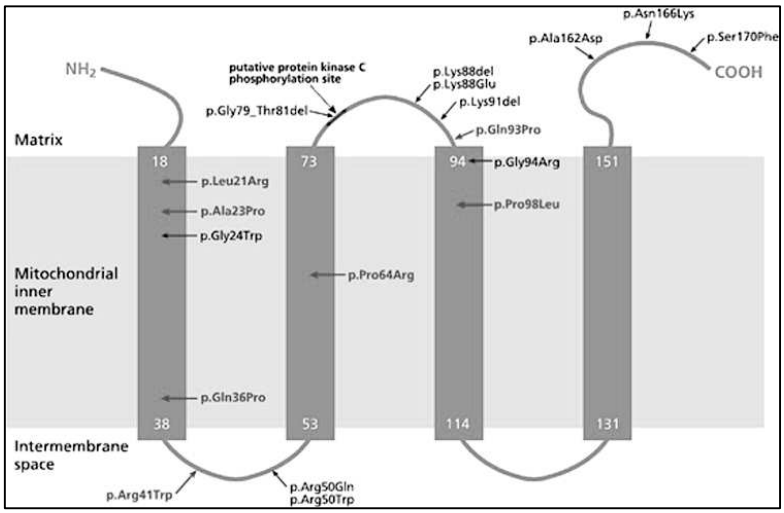

Figure 4. "Schematic representation of human MPV17 protein inside IMM. The 4 α-helical transmembrane spanning domains are indicated by rectangles, and the number of the first and last

amino acids of each of these domains is annotated in white; arrows indicate known point mutations", from Uusimaa *et al.*, 2014.

Importantly, the protein is not processed upon membrane transport or incorporation and seems to miss canonical mitochondrial localization sequences (Spinazzola *et al.*, 2006).

3.2 Clinical features

In humans, different mutations in *MPV17* gene cause either an infantile mtDNA maintenance disorder displaying a spectrum of combined hepatic, neurologic and metabolic manifestations, or produce an adult-onset multisystemic disease with multiple deletions in mtDNA. The typical earliest manifestation of *MPV17*-related MDS is liver dysfunction, including jaundice, cholestasis, coagulopathy and, in some cases, hepatomegaly and cirrhosis. In the vast majority of affected individuals (91%), liver disease progresses to liver failure during infancy or early childhood. Neurologically, affected individuals typically show developmental delay (82%) and generalized hypotonia (74%). Frequently, failure to thrive occurs (90%), as well as metabolic derangements, including lactic acidemia (79%) and hypoglycemia (60%) (El-Hattab *et al.*, 2018). In most cases, liver transplantation represents the main cure for liver failure in this disease, although this therapeutic strategy remains controversial for mitochondrial hepatopathies, largely because of the multi-organ involvement in mitochondrial disorders (Parikh *et al.*, 2016).

From the biochemical point of view, all affected individuals identified so far had a 1% to 40% mtDNA depletion in the liver, while 89% of patients exhibited 8% to 80% mtDNA depletion in muscle, when compared to controls (El-Hattab *et al.*, 2018). The RC activity assays of patients show decreased activity of multiple complexes, I or I + III being the most affected (El-Hattab *et al.*, 2010).

Patients are either homozygotes or compound heterozygotes for *MPV17* mutations, providing genetic evidence for them to be loss of function. Notably, the majority of *MPV17* pathogenic variants has been identified in one or few families, except for the missense mutations c.149A>G (p.R50Q), c. 278A>C (p.Q93P) and c. 293C>T (p.P98L), described in several individuals of various ethnicities (El-Hattab *et al.*, 2018). In particular, p.R50Q substitution was found to be causative of a neurohepatopathy in different Native American Navajo families and has been also discovered to cause the typical *MPV17*-related MDS in some Italian patients (Spinazzola *et al.*, 2006). Its clinical signs perfectly match with the most frequent manifestations of *MPV17*-related hepatocerebral MDS; in fact, patients with Navajo neurohepatopathy (NNH) show liver disease, severe sensory and motor neuropathy, corneal anesthesia and scarring, cerebral leukoencephalopathy, failure to thrive and recurrent metabolic acidosis with intercurrent illness (Karadimas *et al.*, 2006).

3.3 MPV17 function

Controversial information can be found in literature regarding *MPV17* putative function. In 2015, the yeast MPV17 orthologue protein was suggested to play a role in mitochondrial homeostasis as a $\Delta\Psi_m$-modulating channel (Antonenkov *et al.*, 2015), while a work carried out in human fibroblasts by Spinazzola and colleagues in 2016 associated *MPV17* deficiency with dNTP insufficiency, placing *MPV17*-related disease firmly in the category of mtDNA disorders caused by deoxynucleotide perturbation. This hypothesis was also encouraged by works in which MPV17 was suggested to be a dNTP carrier in zebrafish. In particular, the zebrafish *mpv17* (*tra*) *transparent* mutant displays a severe impairment of

iridophores, pigment cells in which the guanine is deposited in crystals (Krauss *et al.*, 2013).

3.4 MPV17 paralogues

MPV17 belongs to a conserved family of integral membrane proteins consisting of four members in mammals: PXMP2 (PMP22), MPV17, MPV17-Like, and FKSG24 (MPV17-Like2). Phylogenic analysis indicates that, before the radiation of the eukaryotes, a gene duplication event created the two *MPV17/Like/Like2* and *PMP22* clades. Later in early metazoans evolution, gene duplication events gave rise to the *MPV17*, *MPV17-Like* (*L*) and *MPV17-Like2* (*L2*) paralogous and the phylogenetic analysis suggests that *MPV17L* and *MPV17L2* are sister groups of each other (Dalla Rosa *et al*, 2014). Pairwise comparisons of amino acid sequences of human *MPV17*-family members show that *MPV17L2* has the highest level of sequence similarity and identity when compared to *MPV17* and that *MPV17L2* and *PMP22* are the closest homologues to *MPV17* (Fig.5).

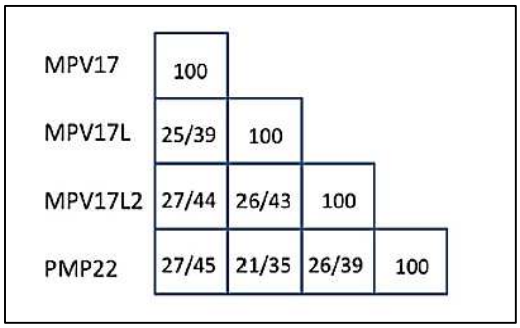

Figure 5. "Levels of sequence identity/similarity among the human MPV17 *family members. The ordering of the proteins along the horizontal axis is identical as that along the vertical axis", from Dalla Rosa et al., 2014.*

On the other hand, *PMP22* is located on human chromosome 12q24.33 and it encodes a peroxisomal protein acting as a non-selective channel, transferring small solutes across the peroxisomal membrane (Rokka *et al.*, 2009). *MPV17L* localizes on human chromosome 16p13.11 and its encoded protein has been controversially found both in peroxisomes, where it upregulates the expression of

Manganese superoxide dismutase by taking part of ROS metabolism (Iida *et al.*, 2003), and in mitochondria, where it may exert antioxidant and antiapoptotic functions (Krick *et al.*, 2008). In contrast to the localization of PXMP2 and MPV17L, MPV17 and MPV17L2 localize specifically to the IMM. *MPV17L2* gene is located on human chromosome 19p13.11 and encodes a 206 amino acids long transmembrane protein. Recent studies suggested that MPV17L2 may contribute to mitochondrial ribosome biogenesis, linking the two ribosomal subunits in order to create the translationally competent monosome. According to these results, MPV17l2 abundance seems to be dependent on mtDNA, since it is absent from ρ^0 cells (cells deprived of mtDNA) (Dalla Rosa *et al.*, 2014).

3.5 Model organisms

As mentioned above, loss-of-function mutations in *MPV17* orthologous genes are known to cause mtDNA abnormalities in different organisms; however, all these models show only few characteristics that resemble human *MPV17*-related MDS.

3.5.1 The *Mpv17* mutant mouse model

In 1990, before the connection between *MPV17* and MDS was established, a knock-out mouse strain was generated by an insertional inactivation with a recombinant retrovirus (Weiher *et al.*, 1990) and later characterized by Viscomi and colleagues (Viscomi *et al*., 2009). The most evident phenotype described in the mouse is a renal disease characterized by focal segmental glomerulosclerosis and consequential nephrotic syndrome. Importantly, in first reports mutant mice died 18 weeks after birth because of renal failure, while in other studies mice survived for 1 or 2 years. In fact, the glomerulosclerosis phenotype changed over time with respect to onset, severity, and lifespan of animals, thus suggesting an

important role in pathogenesis for the genetic background (Lollgen and Weiher, 2014).

In addition, inner ear structures of *Mpv17* mice are degenerated, involving deterioration of the organ of Corti, loss of inner and outer hair cells as well as spiral ganglion cells. Moreover, *Mpv17* KO mice show sensineural hearing loss, progressing to deafness by 2 months of age. It seemed that in glomeruli, *Mpv17* deficiency led to extracellular release of ROS, directly resulting in toxic modifications of cellular components. Interestingly, kidney phenotype can be prevented by the local administration of dimethylthiourea (DMTU) or human *MPV17* expression, indicating a functional equivalence between the orthologues, whose coding regions were found to be conserved more than 90% (Schenkel *et al.*, 1995). Interestingly, *Mpv17*$^{-/-}$ mice did not develop hepatic failure at any age, despite a severe (4% of mtDNA content measured in wild-type controls) mtDNA depletion, resembling the one present in humans (Spinazzola *et al., 2006*). In fact, in contrast with the human condition, the lack of MPV17 was not associated with metabolic dysfunctions of the mouse model, which, for instance, failed to develop hypoglycemia, and showed increased sensitivity to a hepatotoxic compound. Interestingly, Viscomi and colleagues demonstrated a compensatory mechanism, acting at transcriptional level, that keeps cellular respiration comparable to physiological conditions.

3.5.2 The yeast *MPV17* orthologue *SYM1*

The functional orthologue of *MPV17* was identified in *Saccharomyces cerevisiae* in 2004 (Trott and Morano, 2004). Being a heat stress inducible gene, it was named *SYM1* (Stress-inducible Yeast Mpv17). Sym1 shows 48% similarity and 32% identity with Mpv17 and complementation assays confirmed that the two proteins

are functional orthologues (Trott and Morano, 2004). Sym1 localizes into IMM and it has been recently found to form a voltage-dependent channel, closed at physiological membrane potential, permitting the passage of molecules as large as metabolites (Reinhold *et al.*, 2012). Functionally, Sym1 is a heat-shock protein associated with oxidative growth at elevated temperature. In addition, mutants show OXPHOS defects, that can be rescued by supplementation of non-essential amino acids, suggesting a defective production of common intermediates. Hence, the metabolic defect of *sym1Δ* mutant strain is also rescued by two suppressors, namely *YMC1* and *ODC1*, both encoding mitochondrial transporters supposed to transfer TCA cycle intermediates from cytosol to mitochondria, hence supporting the idea that Sym1 might be involved in the homeostatic control of TCA cycle intermediates (Dallabona *et al.*, 2010) (Fig.6).

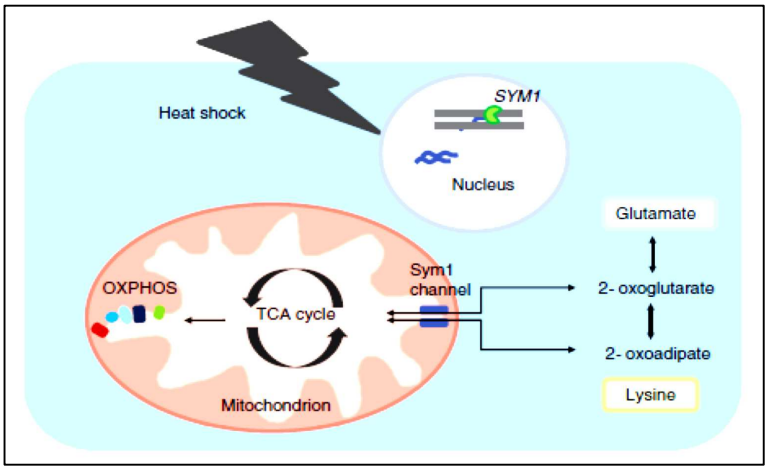

Figure 6. Sym1 role in Saccharomyces cerevisiae. The mechanism proposed by Dallabona *et al.* (2010) suggests that the Sym1 channel may be essential for transport of TCA cycle intermediates in and out of mitochondria. Rescue experiments showed that Sym1 function can be bypassed by the delivery of intermediates through other pathways in *sym1Δ* yeast model (Lollgen and Wehier, 2015).

Another phenotypical feature of *sym1Δ* model is the formation of *petite* colonies at permissive growth conditions. The *petite* phenotype is associated with mtDNA instability (depletion or multiple deletions), which may be the main cause of the

OXPHOS defect. Interestingly, in both stringent and permissive growth conditions, the morphology of mitochondria in *sym1Δ* strain has been found profoundly altered, with mitochondrial ballooning, flattening of cristae and accumulation of electron-dense particles (Dallabona *et al.*, 2010).

3.5.3 The *mpv17* KO zebrafish mutant

3.5.3.1 The zebrafish model

Danio rerio is a tropical freshwater fish, member of the family of Cyprinidae and of the ray-finned fish in the infraclass of Teleostei.

Its natural habitats are rivers of South Asia, mainly northern India, as well as northern Pakistan, Bhutan, and Nepal (Dahm and Geisler, 2006). It is characterized by a distinctive color pattern based on alternating dark and light horizontal stripes: because of this phenotypical tract, it is commonly called “zebrafish”. Female and male are easily recognized because of their sexual dimorphism: while males present a fusiform body shape and a red/goldish coloration on fins and abdomen, females have a more rounded body shape and a yellow/white coloration on the abdomen (Fig.7).

Figure 7. Example of female (the upper one) and male (the lowest one) zebrafish.

Several are the advantages of using zebrafish as a model: for instance, its genome has been completely sequenced; fish can easily and cheaply bred in laboratories all year round; their generation time is short (about three months); fertilization is external and embryos are thus accessible for observation, experimentation, and

drug administration; embryos are optically clear, allowing to follow individual cells during a very rapid animal development (Fig.8).

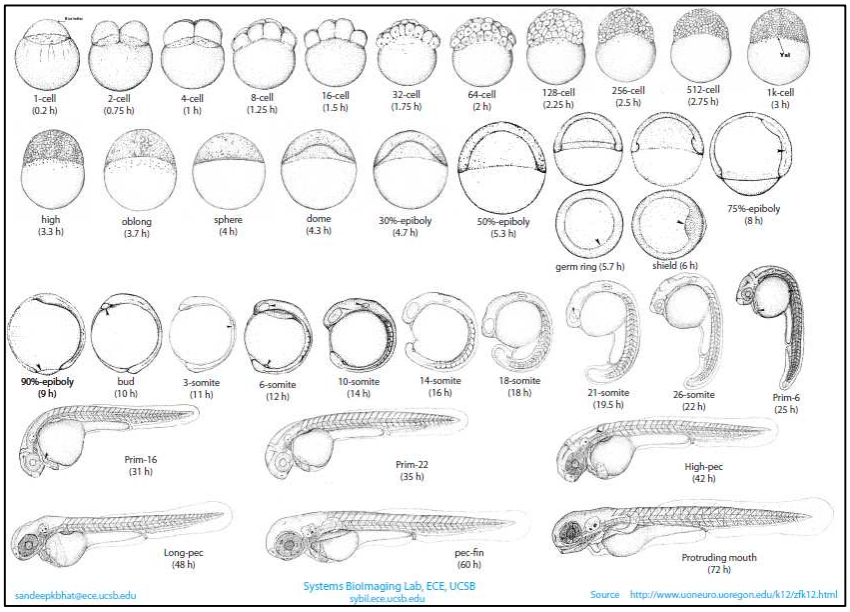

Figure 8. Zebrafish embryo development. Developmental stages from 0.2 hour (1-cell) to 72h post-fertilization (hpf) are showed.

In fact, the blastula stage lasts only 3 hours, gastrulation is completed within 5 hours, and at 24 hours many primary organ systems have formed. In just four days, the embryo has rapidly become a small version of the adult, obviously simplifying developmental and genetic studies.

In addition, even though the evolutionary distance from humans is bigger when compared to other model organisms (*Danio rerio* and humans separated about 420 million years ago), genes and molecular mechanism defining embryonic development are found to be highly conserved in this animal. Moreover, about 80% of genes known to be associated with human diseases have a zebrafish counterpart (Howe *et al.*, 2013).

Given its numerous advantageous characteristics, zebrafish has recently become one of the most prominent vertebrate model organisms to study the genetics underlying development, physiology and disease.

The growing interest in zebrafish research, demonstrated by the continuous increase in zebrafish projects granted and in the publication of papers using zebrafish as model organism (Fig.9), has been paralleled by a constant development of new technologies and tools applied to this model *in vivo*.

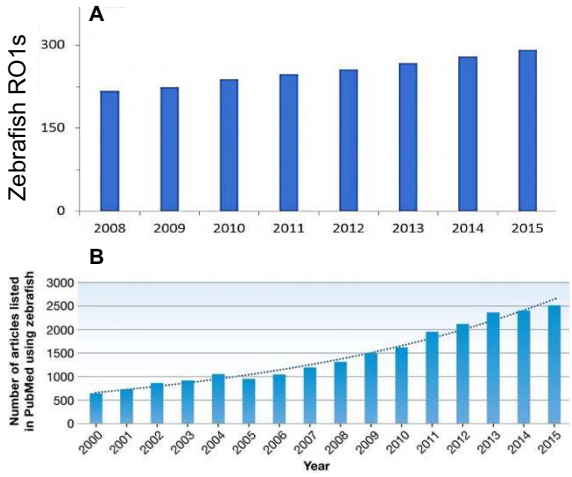

Figure 9. Zebrafish Research Project Grant (RO1) awarded by NIH (A). Annual growth trend of articles using zebrafish in PubMed (B) (Geisler et al., 2016).

In particular, sophisticated protocols for generating mutant and transgenic zebrafish lines have been developed and used to create reporter lines able to reveal *in vivo* signaling pathway or to drive the expression of fluorescent proteins into specific cellular and subcellular structures. In the last years, *Danio rerio* has also been discovered to be very suitable for large-scale drug screenings: all these advantages make zebrafish a useful preclinical model organism for predicting drug effects in humans. This is the case of leflunomide, screened in zebrafish as a new drug against melanoma progression and then entered in clinical trials (White *et al.*, 2011).

3.5.3.2 roy orbison and transparent

The three classes of zebrafish pigment cells - melanophores, iridophores and xantophores - derive from the neural crest, an essential population of cells that gives rise to diverse cell lineages, also including peripheral and enteric neurons.

Two spontaneous zebrafish *mpv17* recessive null mutations, causing *roy orbison* (*roy*) and *transparent* (*tra*) phenotypes, have been independently identified and several evidences strongly support the idea that mutant phenotype might be caused by a similar or even the same allele (D'Agati *et al.*, 2017, Krauss *et al.*, 2013). For instance, it has been previously demonstrated that both mutants lack 19 bp resulting in aberrant splicing between the exons 2 and 3 of *mpv17* (D'Agati *et al.*, 2017, Krauss *et al.*, 2013). Moreover, *roy* and *tra* display, as the most severe phenotypical tract, pigmentation abnormalities due to the lack of iridophores, both in larvae and in adult fish. This lack gives the eye its specific black appearance (vaguely resembling the popular image of the famous rock-and-roll singer Roy Orbison) and it causes a partial transparency of the skin. In fact, even though melanocyte development initially appears normal, adults progressively lose almost completely this class of pigmented cells, possibly as a secondary effect due to the interaction between the two cell types (Fig.10). On the other hand, no defect is observed in xantophores.

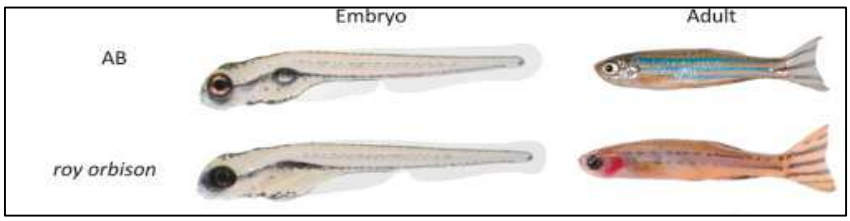

Figure 10. "The roy orbison mutant phenotype: during development, roy nearly lacks all the reflective iridophores, but melanophore development is relatively normal. In contrast, as adult, *roy* shows a severe defect in both iridophores and melanophores, compared to wild-type AB", from D'agati *et al.*, 2017.

In *Danio rerio*, *mpv17* is located on chromosome 20, is composed of eight exons, encodes a 177 residues-long protein and its product has been previously found to localize inside mitochondria (Krauss *et al.,* 2013). In order to prove the genotype-phenotype correlation in *roy*, various experiments have been performed: the injection of zebrafish *mpv17* mRNA in single-cell stage mutant embryos was found to rescue iridophores number at 4 dpf; the silencing of *mpv17* expression, through morpholino injection in wild type embryos, determined either complete or moderate loss of iridophores at 4-7 dpf in 90% of the injected fish. Moreover, new *mpv17* mutant lines, created by using the CRISPR-Cas9 technology, reproduced *roy* phenotype, confirming loss of *mpv17* as the cause of iridophore defect in zebrafish.

The link between Mpv17 and iridophores is to date unclear, primarly because iridophore ontogeny is not well-understood. What is known about these pigment cells is that they produce a large amount of crystals mainly consisting of guanine, localized in subcellular organelles called iridosomes (Fig.11).

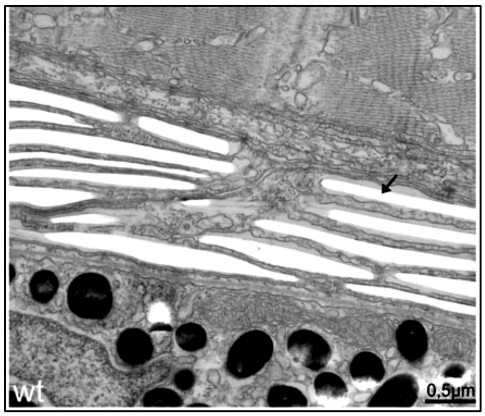

Figure 11. "Electron Microscopy section of wild-type iridophores in the eye of 5 dpf larvae. Iridosomes are not contrasted and appear empty as the guanine crystals are lost during the sectioning process (arrow)", from Krauss *et al.*, 2013.

Recently, iridophore transcriptome has been analyzed and it revealed a dramatic upregulation of specific enzymes from several metabolic pathways that coordinate dNTP transport, as it would be expected (Higdon *et al.*, 2013).

Moreover, the isolated skin of *roy* mutants also showed a decrease in mtDNA compared to controls (D'agati *et al.,* 2017), suggesting a mitochondrial defect and a possible link between *mpv17* and mtDNA maintenance also in *Danio rerio*.

4. CRISPR/Cas9 technology

While zebrafish research initially centered on forward genetics and mutagenesis screens, recent years have seen the establishment of reverse genetic methods (Dahm *et al.*, 2006). In the last 10 years, knockout in zebrafish was totally revolutionized thanks to powerful gene targeting strategies, named sequence-specific nucleases like ZnF, TALENs and the most recent CRISPR-Cas9 system. All these techniques are based on targeted mutations and have already been successfully applied to zebrafish (Hwang *et al.*, 2013; Chang *et al.*, 2013; Cade *et al.*, 2012). In particular, the CRISPR-Cas9 technology is based on an adaptive immunity mechanism of archaea and bacteria, which prevents themselves from being infected by viruses or plasmids. The CRISPR (Clustered Regularly Interspaced Shorts Palindromic Repeats) loci are present in the genome of these groups and are responsible for the acquired immunity. The CRISPR locus is organized in patterns made of palindromic repeats alternate with the protospacer regions, containing a fragment of foreign DNA. This locus is normally located close to that of Cas nuclease (Haft *et al.*, 2005). The invading DNA from viruses or plasmids is cut into small fragments by Cas nucleases and inserted between the short repeats. Then, when the viruses attack a second time, the CRISPR array are

transcribed into CRISPR RNA (crRNA) to guide the nuclease Cas proteins to invasive DNA resulting in its cleavage and degradation, allowing the formation of an adaptive sequence-specific immunity (Marraffini e Sontheimer, 2010; Van der Oost *et al.*, 2014). There are three main types of CRISPR-Cas system: type I that uses helicase-nuclease Cas proteins, type II that uses Cas9 nuclease and type III which uses Cas10 protein, still not well-characterized (Makarova *et al.*, 2015). The system adopted in genetic engineering involves the type II nuclease Cas9, which needs a particular sequence, indispensable for cleavage, near the Protospacer: the so called PAM (Protospacer Adjacent Motif), composed by three nucleotides downstream the target sequence. The Cas9 nuclease presents two regions of interaction: the first cross-talks with the guide-RNA for the positioning in the foreign DNA, whereas the second recognizes the PAM sequence and exerts the exonuclease activity (van der Oost *et al.*, 2014). In this system the guide crRNA has to be processed by a RNase III starting from a duplex composed by the pre-crRNA and a tracrRNA (trans-encoded CRISPR RNA). The most used Cas9 derives from *Streptococcus pyogenes*, and recognises the specific PAM sequence "NGG", from 5' to 3'. To maximize the transport into the nucleus and the efficiency of the mutagenesis, the Cas9 mRNA and its encoded protein contains a Nuclear Localization Sequence (Jao *et al.*, 2013). This technology is simple because a) single sgRNAs are easy to design and synthesize for either single or multiple target loci, and b) it is based on double-stranded breaks (DSBs) produced by Cas9 at the target site, close to PAM sequence, where the enzyme is driven by sgRNAs (Fig.12).

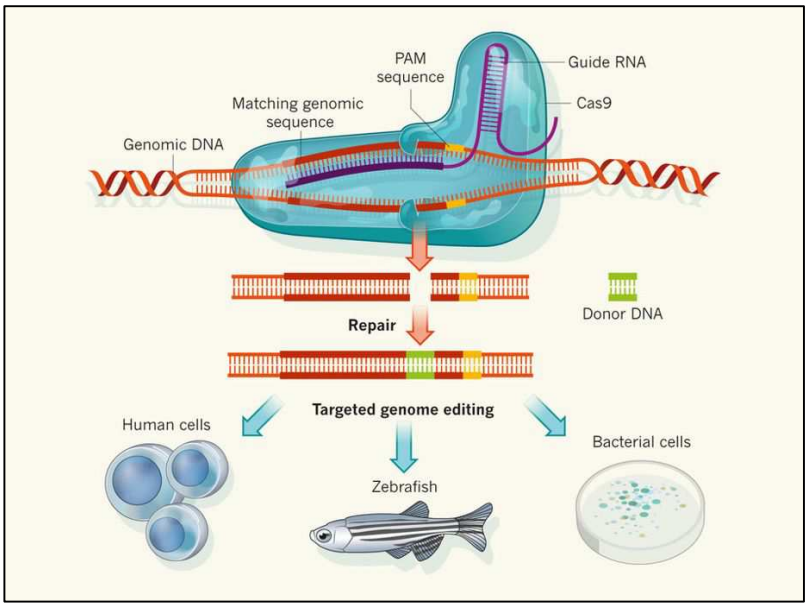

Figure 12. Schematic representation of Cas9 mechanism of action and its application in both in vivo and in vitro models. The enzyme is guided to the target DNA by a RNA molecule that contains a sequence maching the target sequence to be cleaved, which is demarcated by PAM sequences. RNA-guided Cas9 activity creates site-specific double-stranded DNA breaks, which are then repaired. CRISPR/Cas9 technique is largely used in zebrafish model and in human and bacterial cells. (Charpentier and Doudna, 2013)

DSBs can be repaired by error-prone non-homologous end joining (NHEJ) or, if a donor DNA is supplied, by homology-directed repair. Although homology-directed repair tends to be accurate and is generally used for the generation of knock-in alleles, the error-prone NHEJ repair method often leaves insertions or deletions upon repair that are exploited to generate gene knock-outs (Varshney *et al.*, 2016).

Methods

1. Zebrafish husbandry and maintenance

All experiments were performed in accordance with the European and Italian Legislations and with the permission for animal experimentation of the Local Ethics Committee of University of Padova. Zebrafish were maintained in a temperature-controlled (28.5°C) environment and fed as described by *Kimmel et al.*. The *roy orbison* strain was originally obtained from the Harvard Medical School (Boston, USA) and mutants were identified by PCR with the following primers: forward AACCGTTTGTCATAATGTGGC; reverse-wt CATGGGTGTTTGGCCATCAG; reverse-del ACATCAACTACATGGGTGGG.

For *in vivo* studies the following transgenic lines, crossed with *roy orbison,* were used: Tg(*lfabf*:dsRed; *elaA*:EGFP), generated by Korzh *et al.; Tg(SCAC69-mls:EGFP*), generated in our laboratory by Nicola Facchinello, using a construct kindly provided by Seok-Yong laboratory (Chonnam National University Medical School, Gwangju, Republic of Korea) containing the mitochondrial localization sequence of subunit VIII of human cytochrome c oxidase (COXVIII).

2. RNA extraction, reverse transcription and quantitative polymerase chain reaction (qPCR)

Total mRNA was isolated from larvae using Trizol (Invitrogen) and reverse-transcribed using SuperScript® III First-Strand (Thermo Fisher Scientific).

qPCRs were performed using a Rotor-gene Q (Qiagen) and the 5x HOT FIREPol® EvaGreen® qPCR Mix Plus (Solis BioDyne) following the manufacturer's protocol. The cycling parameters were: 95 °C for 14 min, followed by 45 cycles at 95 °C for 15 s, 59 °C for 25 s, and 72 °C for 20 s. Threshold cycles (Ct) and dissociation

curves were generated automatically by Rotor-Gene Q series software. Primers sequences are listed in Table 1. Sample Ct values were normalized with Ct values from zebrafish Glyceraldehyde 3-phosphate dehydrogenase (*z-gapdh*).

Gene	Forward primer (5'-3')	Reverse primer (5'-3')
z-gapdh	GTGGAGTCTACTGGTGTCTTC	GTGCAGGAGGCATTGCTTACA
uqcrc1	ACTCGGCTCACTACCCTAGA	TCAAGAGCAGACTGAGGGTG
mic13	CCCTGTCGTCAAGTTTGC	TCATCCACTCATCCACAG
mic19a	CCTCTTGAATCAGTGGGT	CGTGAGCCTGAGACTTTT
mic19b	CCTCCATTCCCGATTCCT	TCTGCCGTCTTCATCTCC
mic60	CGCTGGGAAAATAGTGGC	TGGTTTGACAGTCTCCGG
mt-cyB	TCTCCACGAAACCGGATCAA	CTAGAGGGTTAGCAGGGGTG
mpv17	TAACTGCTGGCTCTCTGGTG	TGTCCAGCACCTTGTACCAT
mpv17l	CCTCACCTTTGGCGACCA	CCCATGAACGCTGTCCTC
mpv17l2 (ex2)	ATGTTTGCTGTGGGATGCTC	GCGCCTCAATGAAAGTGTGA
mpv17l2 (ex4)	CGATTGGTGTGTTTGGCC	CGGTTCCGTCAGCTTCTTTT

Table 1. Zebrafish gene-specific primers used for RT-qPCR analyses.

3. Whole mount *in situ* hybridization

Whole-mount *in situ* hybridization (WISH) probes for *mpv17-like2* gene were generated as follows: exonic region of *mpv17-like2* gene (ENSDARG00000056367) was polymerase chain reaction (PCR)-amplified from zebrafish cDNA (6 dpf) using the following primers designed by Primer3 software (http://primer3.ut.ee), *mpv17l2* probe-F: GGGAATGATGGAGGGTCACA; *mpv17l2* probe-R: GCCCAGCGTATGTCACAAAT; PCR products were agarose gel-separated and purified, then cloned into pCR2.1 TOPO vector. (TOPO TA Cloning Dual Promoter Kit, Stratagene) and sequence-verified. For riboprobe in vitro transcription, the constructs were linearized with appropriate endonuclease enzyme (Promega) and transcribed with DIG- or FLUO-labelling mix and appropriate RNA polymerase (Roche). For antisense (working) riboprobe, linearization/transcription was performed with NotI/SP6 RNApol. For sense (negative control) probe, linearization/transcription was performed with HindIII/T7

RNApol. *mpv17-l2* riboprobe detection was achieved through NBT/BCIP solution that represents a substrate for the anti-DIG-AP alkaline phosphatase activity producing a visible violet precipitate. WISH was performed on zebrafish larvae at 3 dpf, previously fixed with 4% PFA/PBS and stored in 100% methanol, following standard protocols. At least 20 larvae per condition were processed in a single tube. For signal comparison, control and *roy* larvae were co-processed and co-stained in the same tube; controls were recognized by tail tip excision, performed after PFA-fixation and before WISH.

4. Iridophore count

Iridophores number was measured with the aid of two polarizing filters, basing on the physical property of these cells of being birefringent. Larvae were anesthetized with tricaine (0.16 mg/mL), placed on a glass and the top filter was twisted until it was possible to see the light refracting through the striated muscle. Samples were photographed by using a Leica MDG41 microscope and a Nikon Digital Sight DS Fi2 camera; iridophores were manually counted in the tail region and their amount was normalized to controls.

5. mRNA rescue

The full-length *mpv17* and *mpv17-like2* cDNA from wild-type strain and human *MPV17* cDNA from pCR2.1 TOPO vector, kindly provided by Zeviani laboratory (University of Cambridge, Cambridge, England), were subcloned into the pCS2+ vector using the In-Fusion® HD Cloning Kit (Clontech) and the Clontech online tool for primers design.

The human *MPV17 p.*R50Q (CGG>CAG) mutated form was generated starting from wild-type construct by using Q5® Site-Directed Mutagenesis Kit (New England Biolabs) and the following primers: forward CAGAGAGGCCAGACTCTGACCATG; reverse GTGTTCCTGCAGACCCCG, both designed by NEBaseChanger online tool (New England Biolabs). Capped mRNA was transcribed using the mMessage mMachine® kit (Thermo Fisher Scientific) according to the manufacturer's protocol. The mRNA was resuspended in water and microinjected into 1-cell *roy* embryos at 70 ng/µl. The larvae were scored for rescue of tail iridophores at 3 dpf.

6. Relative quantification of mtDNA content

DNA samples, extracted from 3–10 dpf pooled larvae or sections, were prepared as described by Rahn *et al.* and quantified by PicoGreen assay (Invitrogen) using the Infinite 200 PRO plate reader (Tecan). 8.5 ng of each sample was used in a qPCR reaction and run in triplicate, using 5x HOT FIREPol® EvaGreen® qPCR Supermix (Solis Biodyne). Mitochondrial DNA copy number was determined by the RT-PCR standard curve method using *mt-nd1* as the mitochondrial gene target and the *polg1* gene as a reference for nuclear DNA following the protocol developed by Artuso *et al.* (2012). Delta Ct (dCt) value was calculated by subtracting the Ct of *polg1* from the Ct of *mt-nd1* for each sample.

7. sgRNA synthesis and genotyping of *mpv17-like2* mutants

The *mpv17L2* sgRNAs were designed using CHOPCHOP (Labun *et al.*, 2016) (http://chopchop.cbu.uib.no/index.php). sgRNA sequences are (PAM underlined):

sgRNA1:5′- GGTACCAATAGTGCATGAAGGGG -3′;

sgRNA2: 5′- GGTTGCGTCGCCAACGTTGGGGG -3’.

sgRNAs were synthesized according to Gagnon protocol (Gagnon *et al.*, 2014) using the following primers: sgRNA1: 5′- ATTTAGGTGACACTATA-N20-GTTTTAGAGCTAGAAATAGCAAG -3′; sgRNA2: 5′- ATTTAGGTGACACTATA-N20-GTTTTAGAGCTAGAAATAGCAAG -3′, where N20 indicates sgRNA target sequences without PAM. Animals were genotyped by amplifying the locus using and HOT FIREPol® DNA Polymerase (Solis Biodyne) and the following primers: 5′-GGTGCTTTTGTGTCCTGCAGG-3′, reverse 5′-CCCAAAAAGTACCAGGCCCCC-3’. PCR conditions were as follows: 15min at 95°C; 35 cycles at 95°C for 30s, 62°C for 30s and 72°C for 11s; 72°C for 5s. The resultant PCR amplicons were electrophoresed on a 15% polyacrylamide gel (Invitrogen) to perform heteroduplex mobility assay (Zhu *et al.*, 2014). For verification, PCR products from fish harbouring in/del mutations were subjected to sequencing (BMR Genomics). Poly Peak Parser so ware (http://yosttools.genetics.utah.edu/PolyPeakParser/) was used for identification and sequence characterization of heterozygous mutant carriers generated by genome editing.

8. Transmission Electron Microscopy analysis

Larvae were anesthetised with tricaine (0.16 mg/mL) and fixed with 2.5% glutaraldehyde in 0.1 M sodium cacodylate buffer, then dehydrated, embedded in epoxy resin and sectioned following a standard TEM sample preparation protocol. All steps after fixation were performed by the TEM service of the Department of Biology (University of Padova).

9. Confocal analysis and mitochondrial volume measurements

Double transgenic fluorescence of Tg(*lfabf*:dsRed; *SCAC69-mls:EGFP*) in *roy* background was visualized under a Leica M165FC dissecting microscope and then with a Nikon C2 H600L confocal microscope. Larvae were anesthetised with tricaine (0.16 mg/mL) and then mounted in 1% low-melting agarose gel. Mitochondrially targeted EGFP and dsRed fluorescence was visualized by using 488 and 561 nm lasers, through a 40x immersion objective (Nikon). All images were analysed with Fiji software-64. Mitochondria were automatically segmented on the EGFP fluorescence image stacks, inside dsRed fluorescent mask identifying hepatic tissue, and total mitochondrial volume was calculated. After confocal acquisition, heterozygous and homozygous siblings were genotyped by PCR on DNA previously extracted from single larva as described by Gagnon *et al.* (2014).

10. Haematoxylin-eosin staining

Zebrafish larvae were collected at 6 dpf, anesthetized and then fixed overnight in 4% paraformaldehyde in PBS at 4°C. For histology, 7 µm thin paraffin sections were cut by using a Rotary one (LKB) microtome and stained with haematoxylin and eosin, according to standard protocols. Images were detected using a Leica DMR microscope equipped with a Leica DFC7000T digital camera.

11. Measurement of oxygen consumption rate (OCR)

OCR was measured on zebrafish larvae at 96 hours post fertilization (hpf) with a Seahorse XF24 extracellular flux analyser. Larvae were placed into the XF24 microplate well (1 larva per well) and blocked with a capture screen in the presence

of 670 µL of fish water (0.5 mM NaH_2PO_4, 0.5 mM $NaHPO_4$, 3 mg/L instant ocean). The basal respiration was measured for 63 minutes at 28.5 °C, while the maximal respiration was measured upon FCCP 0.5 µM. A mixture of 2 µM rotenone (Rot) and 5 µM antimycin A (AA) was added to shut down electron transport chain function, revealing the non-mitochondrial respiration. Basal respiration was obtained by subtracting non-mitochondrial respiration. Respiratory rates are average±SEM of at least 20 individual larvae per condition.

12. Western blot analysis

Proteins were extracted from larvae at 6 dpf. Lysis was performed in ice-cold RIPA buffer (125 mM NaCl, 25 mM TRIS-Cl pH 7.4, 1 mM EGTA-TRIS pH 7.4, 1% Triton-X100, 0.5% sodium deoxycholate, 0.1% SDS and Complete EDTA-free protease inhibitor cocktail (Roche) on ice. Crude lysate was cleared by centrifuging 30 min at 13,200 rpm and proteins in the supernatant quantified using the BCA Protein Assay Kit (Pierce). Equal amounts of proteins (50 µg) were loaded on 4-12% Bis-Tris NuPage gels (Life Technologies) SDS/PAGE and blotted on PVDF Immobilon-P membranes (Millipore). Dried membranes were then washed with TBS buffer (Tris–HCl 50 mM pH 7.5, NaCl 50 mM) with 1% (w/v) bovine serum albumin (BSA, Sigma) and incubated over night with the indicated primary antibodies at 4°C: Mitoprofile® Human WB Total Oxphos cocktail antibody 1:100 (Abcam ab110411); GRP 75 antibody 1:1000 (Santa Cruz Biotechnology H-155) 1:1000; Actin antibody 1:1000 (Santa Cruz Biotechnology AC-15); Tomm20 antibody 1:10000 (Sigma-Aldrich HPA011562). Secondary HRP-conjugated antibodies (Bio-Rad) were incubated for 1 h at room temperature and protein bands detected by

chemiluminescence on a UVITEC Alliance Mini HD9. Quantitation of the signal was performed with ImageJ.

13. Compound administration

Deoxynucleotide Set (SLBH8759), Orotic acid (O2750) and L-Dihydroorotic acid (D7128) were obtained from Sigma-Aldrich. dNTPs (12.5 µM each) were added to embryo medium at 8 hpf, while Orotic acid (1 µM) and L-Dihydroorotic acid (100 µM) were injected into the yolk sac of 20 hpf embryos as described by Willer *et al.*. Controls were injected at 20 hpf, respectively, with a control solution containing NaOH or DMF and phenotypic rescue was evaluated at 3 dpf.

14. Statistics

GraphPad software (GraphPad Software Inc.) was used for data analysis and figure plottings. All experiments were performed at least in triplicate. Standard error of the mean calculations and all statistical analyses were performed by using Mann-Whitney unpaired non-parametric test.

Results

1. Investigation of the role of *mpv17* orthologue and paralogue genes

1.1 *roy orbison* mild phenotype may be due to genetic compensation

Zebrafish *mpv17* null mutants are viable and fertile, not displaying any evident difference in lifespan or tissue functionality.

Since the apparently mild phenotype we observed could be due to several compensatory mechanisms taking place for adaptive reasons by the upregulation of gene families paralogue (Rossi *et al.*, 2015), we wondered if *roy* showed any overexpression of *mpv17* paralogous genes.

As mentioned before, in humans two *MPV17* paralogues, *MPV17L* and *MPV17L2*, are known to be localized inside mitochondria (Krick *et al.*, 2008 and Dalla Rosa *et al.,* 2014) and are both conserved in *Danio rerio*.

Interestingly, by performing RT-qPCR analysis, we observed a significant overexpression of *mpv17l*2, while *mpv17l* expression level remained unchanged in both wild-type and homozygous larvae at 6 dpf (Fig.13).

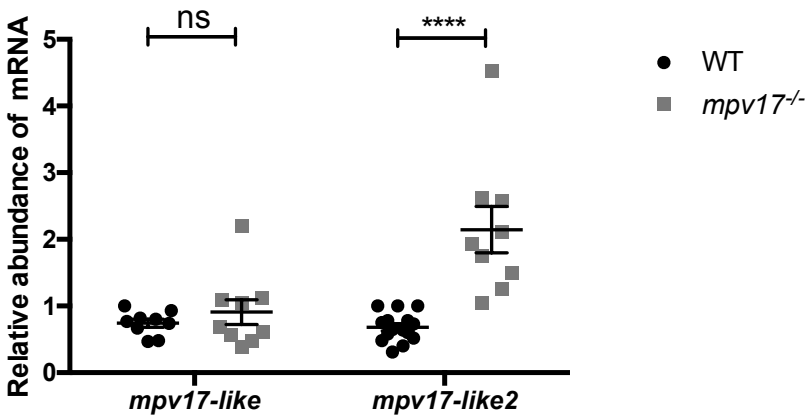

Figure 13. Real-time qPCR quantification of mRNA transcripts of mpv17 paralogue genes, mpv17l and mpv17l2, at 6 dpf. Statistical analyses were performed by using Mann-Whitney unpaired non-parametric test. The statistical significance was evaluated by setting a confidence interval of 95%. The p values were set as follows: ****=p<0.0001; ns=not significant.

In order to confirm the overexpression of *mpv17l2* gene we detected in *roy*, we decided to perform whole mount *in situ* hybridization on wild-type and *roy orbison* larvae at 3 dpf (Fig.14).

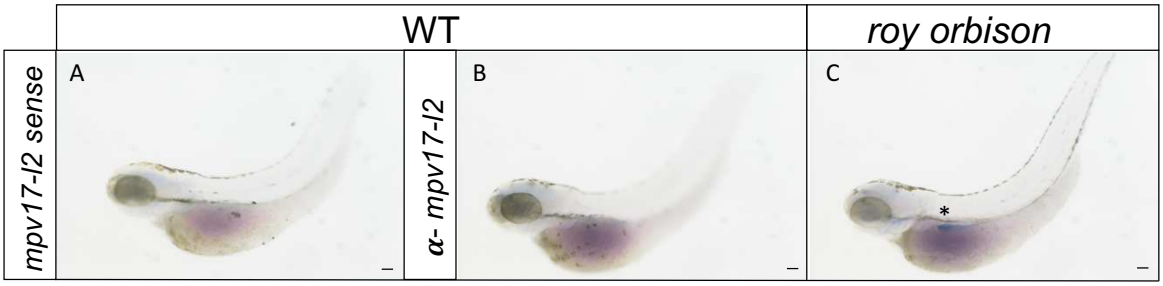

Figure 14. Expression analysis of zebrafish mpv17-l2 gene on wild-type and roy orbison larvae at 3 dpf. (A) Absence of *mpv17-l2* signals in wild-type incubated with sense and (B) antisense probe. (C) The *mpv17-l2* signal is detected in *roy orbison*. Asterisk points to *mpv17-l2* expression region in liver and intestine (blue signal). Bars, 100 µm.

Interestingly, by comparing *roy* and wild-type controls, we observed a clearly detectable overexpression of *mpv17l2* gene in *roy orbison*, while the signal was almost totally absent in wild-type larvae. Moreover, *mpv17l2* expression pattern appears highly specific and restricted to liver and intestine tissues.

These data strongly suggest *mpv17l2* as an important player in ameliorating *mpv17* mutant phenotype, considering the high sequence identity between these paralogues and their common mitochondrial localization.

1.2 *mpv17-like2* and *hMPV17* mRNAs increase iridophores number in *mpv17* null mutants

As we found a specific *mpv17l2* upregulation in *mpv17* null mutant larvae, we decided to check whether a higher amount of *mpv17l2* transcript might transiently rescue *roy* phenotype and if protein functions could overlap.

Moreover, taking into account the high percentage of identity between zebrafish and human MPV17 orthologous proteins and that *p.*R50Q missense mutation is known to cause Navajo neurohepatopathy (Karadimas *et al.*, 2006), we verified their functional homology by performing rescue experiments. In fact, early phenotyping of zebrafish *mpv17* mutants can be easily performed with the aid of a microscope equipped with two polarizing filters and using the birefringence property of iridophores, readily visible at 3 dpf (Higdon et al., 2013). In fact, superficial iridophores are the first metamorphic chromatophores becoming observable in the dermis of the lateral trunk at early stages of development. They appear only later in the anterior trunk in a segmental fashion, continuing to increase in number and to accumulate to form the first ventral inter-stripe (Frohnhöfer *et al.*, 2013). We therefore injected mRNAs encoding zebrafish Mpv17, Mpv17l2 and human MPV17, respectively in a wild-type and a *p.*R50Q mutant form, in *roy* at one-cell stage and we looked at iridophore phenotype (Fig.15).

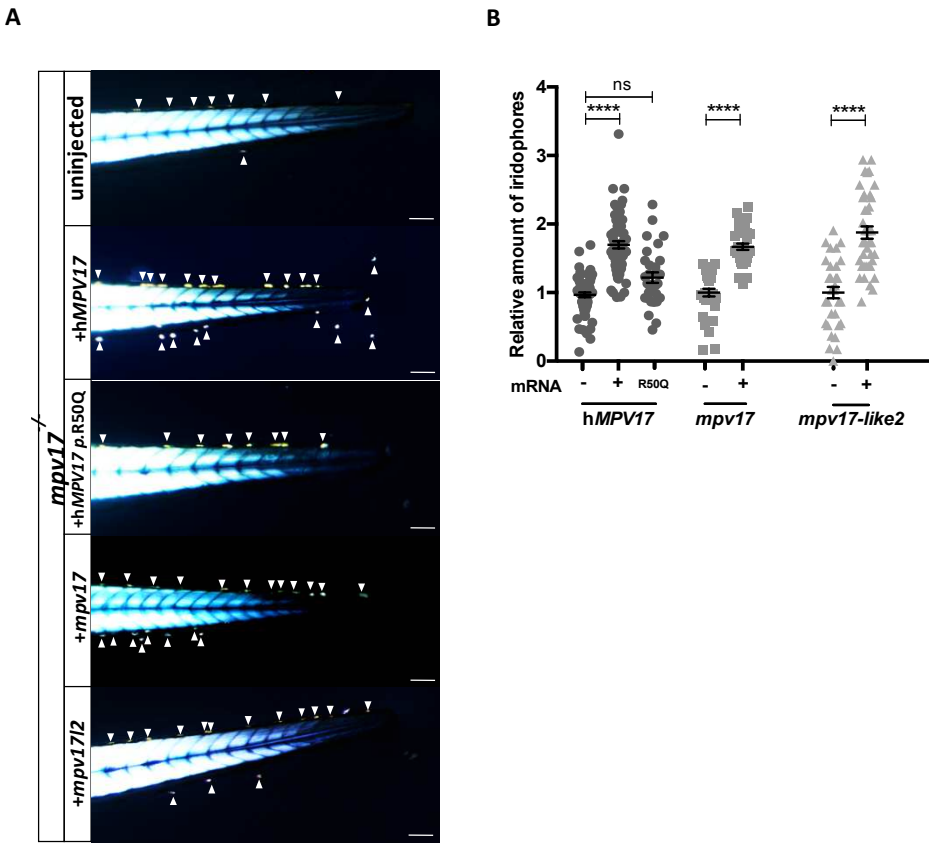

Figure 15. Evaluation of phenotypic rescue in the tail region after the injection of human MPV17, in wild-type and p.R50Q mutated forms, zebrafish mpv17 and mpv17l2 mRNA (A) and relative quantification of iridophore amount (B). The arrows point to iridophores. Bars, 100 µm. Statistical analyses were performed by using Mann-Whitney unpaired non-parametric test. The statistical significance was evaluated by setting a confidence interval of 95%. The p values were set as follows: ****=p<0.0001; ns=not significant.

Interestingly, we observed a significant and comparable increase in iridophores number in all injected larvae, except for embryos injected with *hMPV17* mutant mRNA. These data strongly indicate that one of the most frequent *MPV17* mutation is non-functional also in zebrafish model, validating *roy orbison* as a model for studying *MPV17*-related MDS and Navajo neurohepatopathy.

In addition, given that *mpv17l2* transient overexpression ameliorated iridophore phenotype in *roy orbison*, we also decided to investigate whether or not it might also play a role in increasing mtDNA copy number (Fig.16).

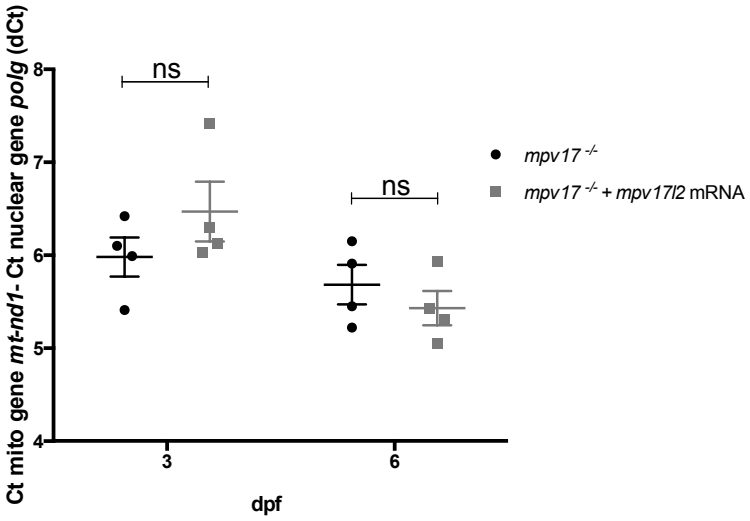

Figure 16. mtDNA copy number analysis in roy transiently overexpressing mpv17l2 at 3 and 6 dpf. Mean dCt values were calculated as Ct of mt-nd1 (mitochondrially-encoded gene) minus Ct of polg1 (nuclear gene) and plotted with SEM. Statistical analyses were performed by using Mann-Whitney unpaired non-parametric test. The statistical significance was evaluated by setting a confidence interval of 95%. ns=not significant.

By performing mtDNA content analysis on injected embryos, we found a non-significant increase in mtDNA content at 3 dpf and no differences at 6 dpf, suggesting that *mpv17l2* transient overexpression does not have a significant effect on mtDNA maintenance at this stage of larval development. Unfortunately, *mpv17l2* mRNA injection increases Mpv17l2 protein amount only for few days and we were not able to follow its effects at later time points.

All these data together show that *mpv17* and *mpv17l2* functions partially overlap and also demonstrate the high similarity between human and zebrafish mpv17 orthologues, confirming *roy orbison* as a potential tool for investigating *mpv17* conserved function, to date unclear.

1.3 Generation of a zebrafish *mpv17-like2* mutant line

As we previously observed that *mpv17l2* is physiologically upregulated in *roy orbison* and, moreover, its transient overexpression significantly ameliorated

mpv17 null mutant phenotype at iridophore level, we decided to generate a *mpv17l2* mutant line by CRISPR/Cas technology.

To date, no zebrafish mutants lacking Mpv17l2 are available and we wondered whether the loss of this paralogous protein, highly similar to *mpv17*, was able to cause a phenotype similar to the one observed in *roy orbison*.

Thus, taking into account that zebrafish *mpv17l2* is a small gene composed of five exons and encoding a 199 aa protein with no predicted splicing variants, we synthesized different sgRNAs targeting exon 2 to generate an early stop codon and a truncated protein. In particular, we selected the two sgRNAs designed by CHOPCHOP website with the highest scores (Fig.17).

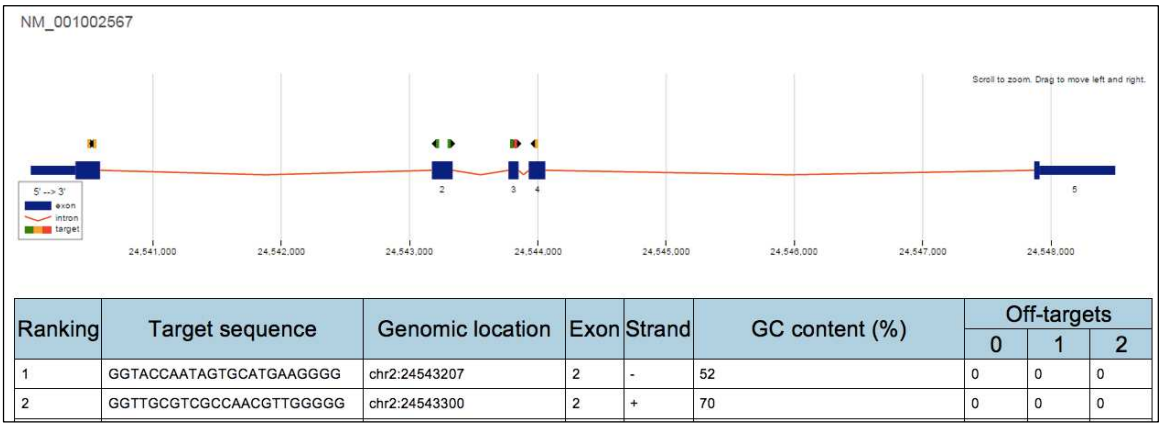

Ranking	Target sequence	Genomic location	Exon	Strand	GC content (%)	Off-targets		
						0	1	2
1	GGTACCAATAGTGCATGAAGGGG	chr2:24543207	2	-	52	0	0	0
2	GGTTGCGTCGCCAACGTTGGGGG	chr2:24543300	2	+	70	0	0	0

Figure 17. Output of CHOPCHOP website (http://chopchop.cbu.uib.no) for mpv17l2 sgRNAs design.

After the co-injection of sgRNA#1 and NLS-Cas9, by performing heteroduplex mobility assay (HMA) we isolated different founders, respectively displaying deletions of 1, 3 and 7 bp in exon 2.

Particularly, we decided to focus on 7 bp deletion (Δ7), predicted to cause an early stop codon in position 90/199 aa and we isolated heterozygotes individuals in F_1 generation (Fig.18).

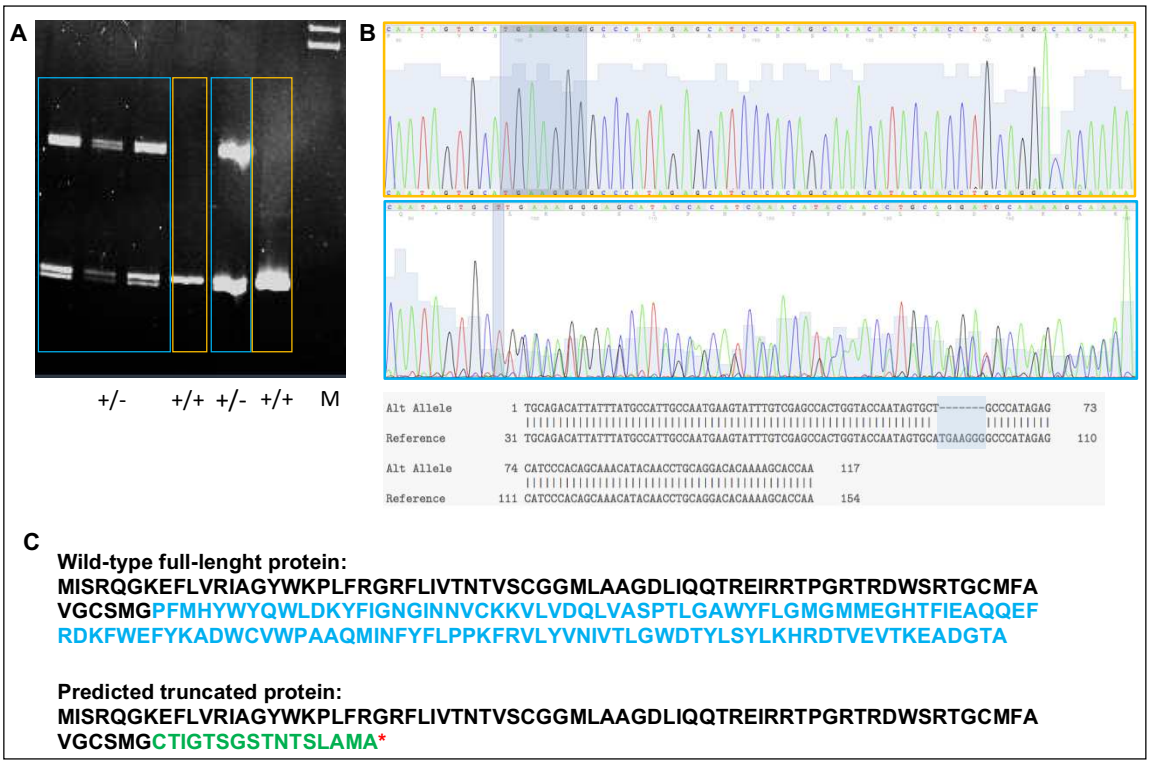

Figure 18. Genotyping and sequencing of mpv17l2 F_1 mutants. HMA on PCR amplicones using DNA extracted from *mpv17l2* Δ7 heterozygotes and wild-type siblings. M=marker (A). Output of poly peak parser website (http://yosttools.genetics.utah.edu/PolyPeakParser/) comparing wild-type (yellow) and heterozygote (turquoise) sequences obtained from PCR sequencing. A deletion of 7 bp is highlighted (B). Sequence of wild-type and predicted truncated Mpv17l2 protein. Aminoacid sequence changes from position 75 to position 90 (turquoise and green). *=early stop codon (C).

Next we out-crossed adult heterozygotes, all displaying no phenotypical differences compared to wild-type siblings, and we better characterized *mpv17l2* Δ7 homozygous mutants. Interestingly, *mpv17l2* Δ7 homozygous mutants reach adulthood, are viable and fertile. Thus, we were able to validate and characterize this mutant line by in-crossing homozygous adults.

1.4 *mpv17-like2* Δ7 mutants show mRNA decay

First of all, to validate *mpv17l2* Δ7 mutant line we verified if nonsense-mediated mRNA decay (NMD) takes place. NMD is a conserved mRNA quality control mechanism that ensures the fidelity of gene expression by detecting and degrading mRNAs containing premature translation termination codons (Wittkopp *et al.*,

2009). This protective event prevents the translation of potentially harmful truncated proteins, leading to a complete loss of the dysfunctional protein. Thus, we extracted RNA from wild-type and homozygous pooled larvae at 6 dpf and we evaluated the total amount of *mpv17l2* mRNA by performing RT-qPCR analysis (Fig.19).

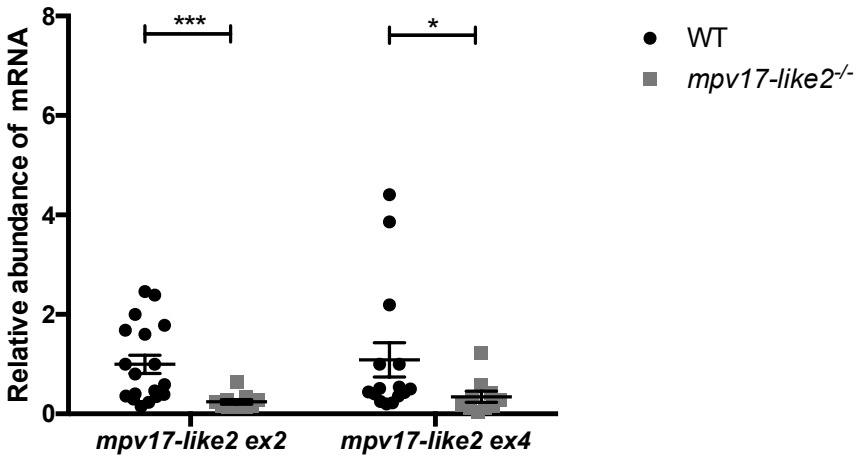

Figure 19. Real-time PCR quantification of mpv17l2 mRNA using different primers, respectively designed in exon 2 and exon 4, on wild-type and mpv17l2 Δ7 homozygous mutants at 6 dpf. Statistical analyses were performed by using Mann-Whitney unpaired non-parametric test. The statistical significance was evaluated by setting a confidence interval of 95%. The p values were set as follows: ***=p<0.001; **= p<0.01.

Consistently, we found a statistically significant reduction of *mpv17l2* transcript levels in *mpv17l2* homozygous mutant, suggesting that the generated deletion of 7 bp induces a premature degradation of *mpv17l2* transcript and, thus, the loss of Mpv17l2 protein.

1.5 *mpv17-like2* Δ7 mutants do not display any overt phenotype

After different out-crosses, we evaluated *mpv17l2* mutant phenotype. Homozygous mutants reach adulthood, are fertile and apparently with no phenotypical feature. Although *mpv17* null mutants display clear defects in neural crest development and pigmentation, we observed no morphological differences both at larval (Fig.20) and

adult stage (data not shown) in *mpv17l2* Δ7 homozygous mutants, compared to wild-type.

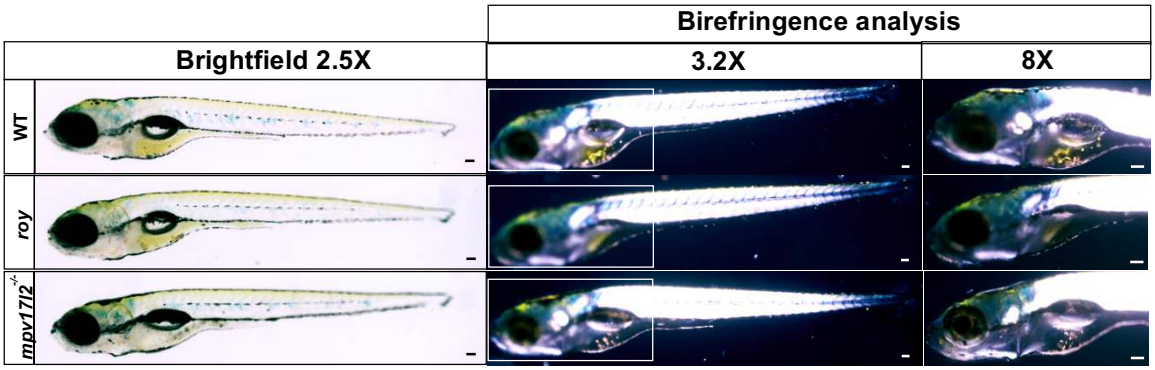

Figure 20. Pictures of mpv17l2 Δ7 homozygous mutants, roy orbison and wild-type larvae at 6 dpf. The panel shows brightfield and birefringent pictures of larvae at different magnifications, with a focus on anterior trunk region. Birefringence analysis was performed with the aid of two polarizing filters and based on the physical property of iridophores of being birefringent. Bars, 100 µm.

In addition, we also wanted to test the hypothesis of a possible upregulation of *mpv17l2* paralogue genes in homozygous mutants, which might justify the absence of a macroscopical phenotype. We therefore performed a RT-qPCR analysis on homozygous and wild-type larvae at 6 dpf, in order to quantify *mpv17* and *mpv17l* mRNA levels (Fig.21).

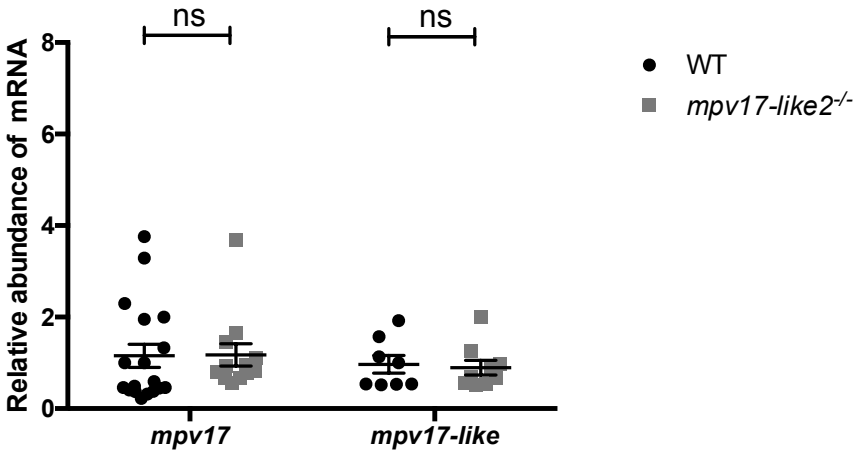

Figure 21. Real-time PCR quantification of mpv17 and mpv17l transcripts in wild-type and mpv17l2 Δ7 homozygous mutants at 6 dpf. Statistical analyses were performed by using Mann-Whitney unpaired non-parametric test. The statistical significance was evaluated by setting a confidence interval of 95%. ns=not significant.

Our data showed no differences in *mpv17l2* paralogue gene expression, thus enhancing the idea of an only partial overlapping function between Mpv17l2 and Mpv17 in zebrafish.

2. Characterization of a *mpv17* KO zebrafish mutant

2.1 The *mpv17* null mutant lose integrity of mitochondria ultrastructure in liver hepatocytes

The spontaneous *mpv17* KO mutant was previously characterized starting from its most evident phenotypical feature: the loss of iridophores.

Considering that zebrafish *mpv17* is known to be a mitochondrial protein (Krauss *et al.*, 2013), we wondered if its absence might affect the structure and functionality of mitochondria.

Firstly, considering that Mpv17 is suggested to be a channel localized into the inner membrane where Mpv17 protein family is thought to be implicated in the maintenance of mitochondrial homeostasis (Antonenkov *et al.*, 2015), we decided to look at *roy* mitochondrial ultrastructure.

By performing Transmission Electron Microscopy analysis, we analysed different sections of liver (Fig.22), muscle and brain tissues (data not shown) at 6 dpf.

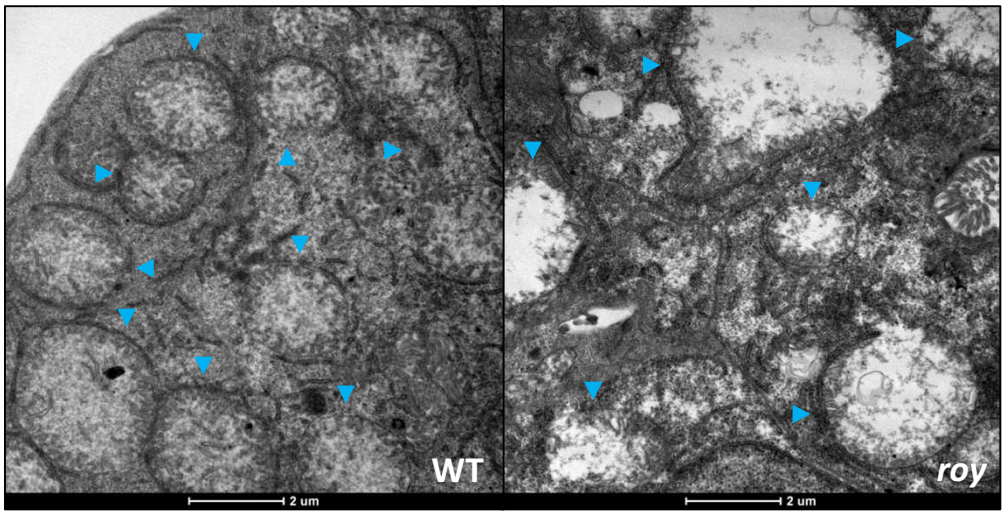

Figure 22. Transmission Electron Microscopy analysis of mitochondrial ultrastructure in wild-type and roy hepatocytes at 6 dpf. The arrows point to mitochondria.

Interestingly, we found a deep alteration of mitochondrial ultrastructure in *roy* liver hepatocytes: in fact, we observed severe mitochondrial ballooning and cristae disappearance, both evidences of disruption of mitochondrial morphology. On the other hand, these alterations were not confirmed at 3 dpf (data not shown) and were specifically found in liver hepatocytes, suggesting that the loss of mitochondrial ultrastructure is a tissue-specific progressive damage, caused by the loss of Mpv17. Interestingly, these data by identifying an overt mitochondrial phenotype in *roy orbison* highlight the important role for Mpv17 in the maintenance of mitochondrial structure.

2.2 Mitochondrial ultrastructure defects of *roy* do not affect mitochondrial volume and tissue integrity in the liver

Since we found severe mitochondrial ultrastructure defects in *mpv17* null mutant larvae, we wondered whether these strong alterations might have any effect on mitochondrial volume in liver tissue. Therefore, we crossed *roy* with two transgenic

lines, respectively expressing a ubiquitous mitochondrially targeted EGFP and a cytosolic dsRed protein under the control of a hepatic promoter. By confocal microscopy we were able to measure total mitochondrial volume inside liver tissue and to compare heterozygotes and homozygous siblings, genotyped after image acquisition (Fig.23).

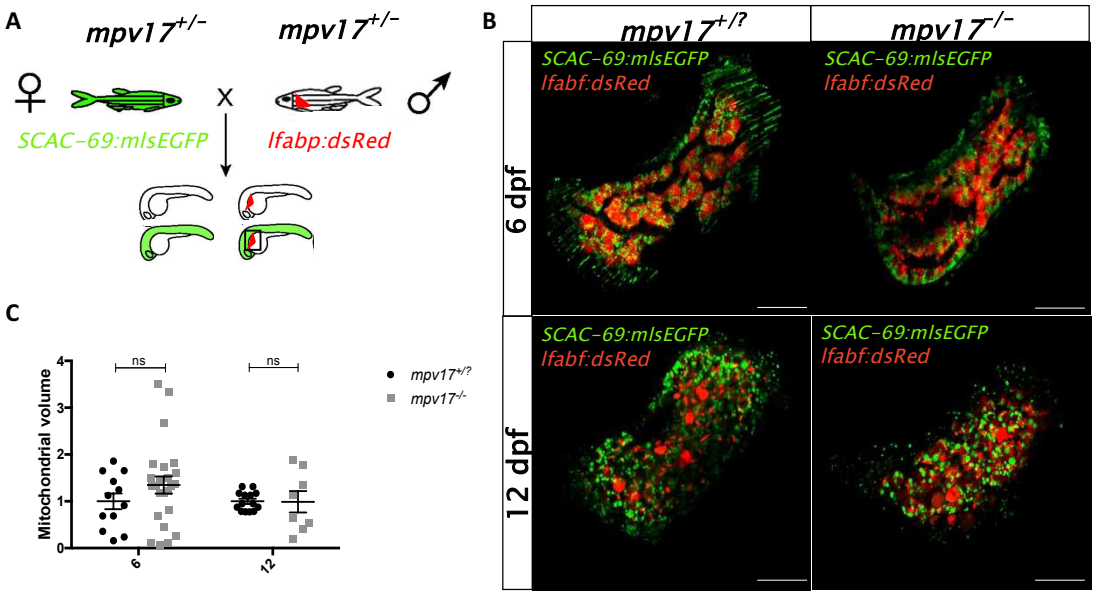

Figure 23. Scheme of mitochondrial volume measurement experiment (A). Confocal images of double Tg(pSCAC-69:mlsEGFP); Tg(ifabp:dsRed) mpv17$^{+/?}$ and mpv17 $^{-/-}$ siblings at 6 and 12 dpf (B) and relative quantification of integrated density (C). Bars, 50 µm. Statistical analyses were performed by using Mann-Whitney unpaired non-parametric test. The statistical significance was evaluated by setting a confidence interval of 95%. ns=not significant.

Our results showed no differences between our samples both at 6 and 12 dpf, suggesting that the loss of mitochondrial ultrastructure does not trigger any obvious mechanism of mitochondrial synthesis and/or recycle at these time points. At the same time, no differences were found in liver volume and integrated density of dsRed fluorescence, meaning that, at these selected time points, loss of Mpv17 does not cause general effects in liver morphology and tissue organization at macroscopical level. In addition, this technique is not able to measure

mitochondrial turnover, thus the balance between mitophagy and mitochondrial biogenesis.

We also wanted to confirm liver tissue integrity in *roy orbison* by performing whole-mount Hematoxylin/Eosin staining at 6 dpf (Fig.24).

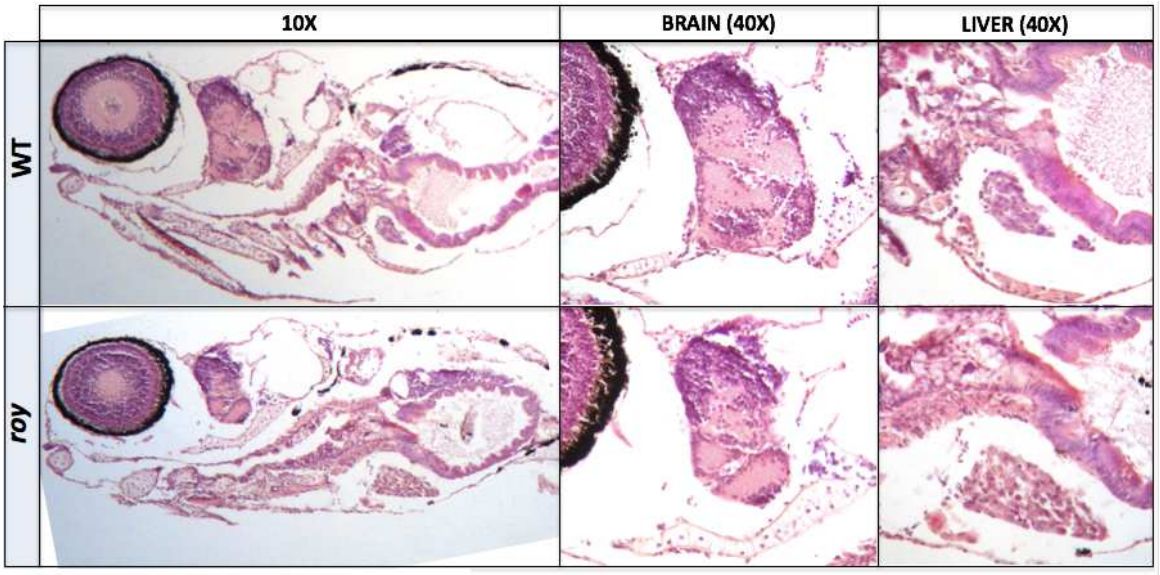

Figure 24. Representative images of 6 dpf roy and wild type sections stained with the HE method. Pictures were acquired at different magnification. Basophilic substances are stained in dark blue-violet, while eosinophilic structures are stained in red-pink.

No marked tissue alterations were detected in *roy* liver at 6 dpf, suggesting that the previously reported mitochondrial ultrastructure loss was not associated with a morphological alteration of *roy* liver at this stage of development.

2.3 Respiratory complexes are impaired in *roy orbison*

Respiratory complexes (RC) localise inside IMM, where they are co-assembled into higher-ordered supercomplexes; mitochondrial cristae disruption is known to impair supercomplex localization and functionality (Stuart, 2008).

Considered the strong mitochondrial ultrastructure alteration detected in *roy* larvae, we tested the hypothesis of a defective OXPHOS functionality in *mpv17* null

mutants. Taking advantage of an *in vivo* assay able to measure Oxygen Consumption Rate (OCR), before and after the addition of inhibitors, we were able to quantify several parameters of mitochondrial respiration. To this aim, baseline OCR is first measured and Basal Respiration (BR) can be derived by subtracting non-mitochondrial Respiration (nmR) from baseline OCR. Addition of carbonyl cyanide-p-trifluoromethoxyphenyl-hydrazon (FCCP), a protonophore, by collapsing the inner membrane gradient allows the ETC to function at its maximal rate and to measure the maximal respiratory capacity by subtracting nmR from the FCCP rate. Lastly, when antimycin A (AA) and rotenone (Rot), respectively inhibitors of complex III and I, are added to shut down ETC function, the nmR is revealed (Rose *et al*., 2014). We therefore decided to perform OCR measurement in *mpv17* homozygous mutants, compared to wild-type controls at 4 dpf (Fig.25).

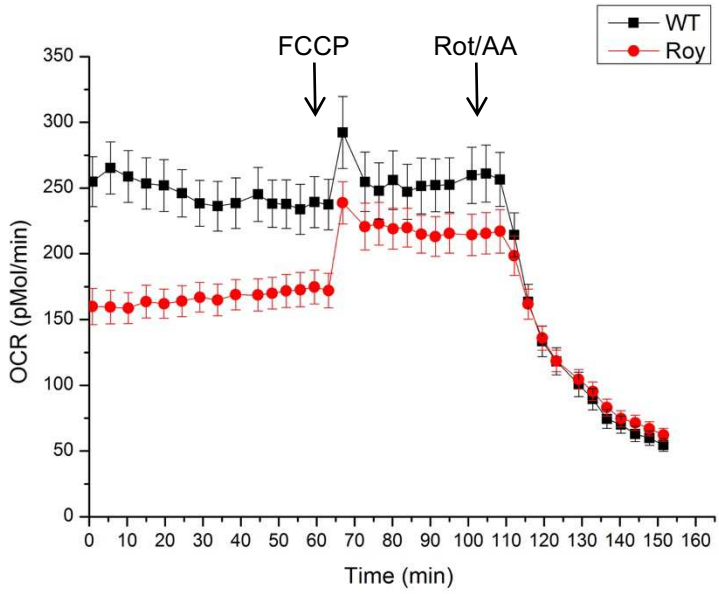

Figure 25. Measurement of OCR in wild-type and roy larvae at 4 dpf. Basal OCR was measured ~1 hour in fish water, immediately after larvae were exposed to 0.5 µM FCCP and, later, to a combination of 2 µM Rot and 5 µM AA. Values represent means ± SEM for four independent experiments.

Interestingly, in the first ~60 minutes, *roy* larvae display a very different OCR pattern, compared to wild-type. In particular, we evaluated basal respiration, before Rot/AA administration, in both *roy* and controls (Fig.26).

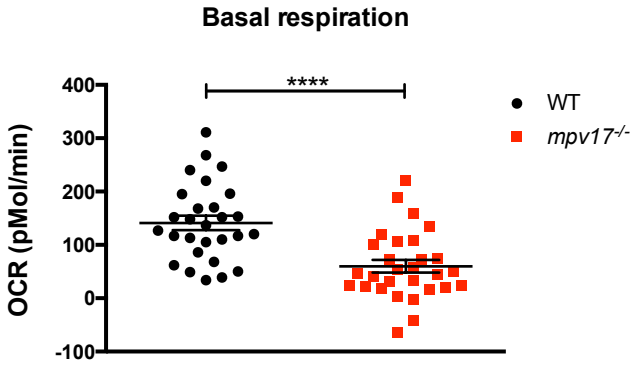

Figure 26. Quantification of basal respiration in wild-type and *mpv17*$^{-/-}$ mutants. Basal respiration was obtained by subtracting nmR (measured upon Rot/AA administration). Values represent means ± SEM for four independent experiments.

These results demonstrated OXPHOS impairment in *roy orbison* larvae at 4 dpf, thus suggesting a defect in energy production and an impaired RC complex activity.

Since previous works showed that in some cases RC assembly steps occur in the inner boundary membrane of cristae (Stoldt *et al.*, 2018), we checked if the amount of RC subunits was affected, by performing western blot analysis on pooled larvae at 6 dpf. We selected this time point taking into account the results from TEM analyses, which clearly identified a strong mitochondrial phenotype at 6 dpf. We used a cocktail of antibodies able to detect all different subunits of OXPHOS complexes and then calculated the total amount of each subunit per cell, by using **β**-actin as normalizer (Fig.27).

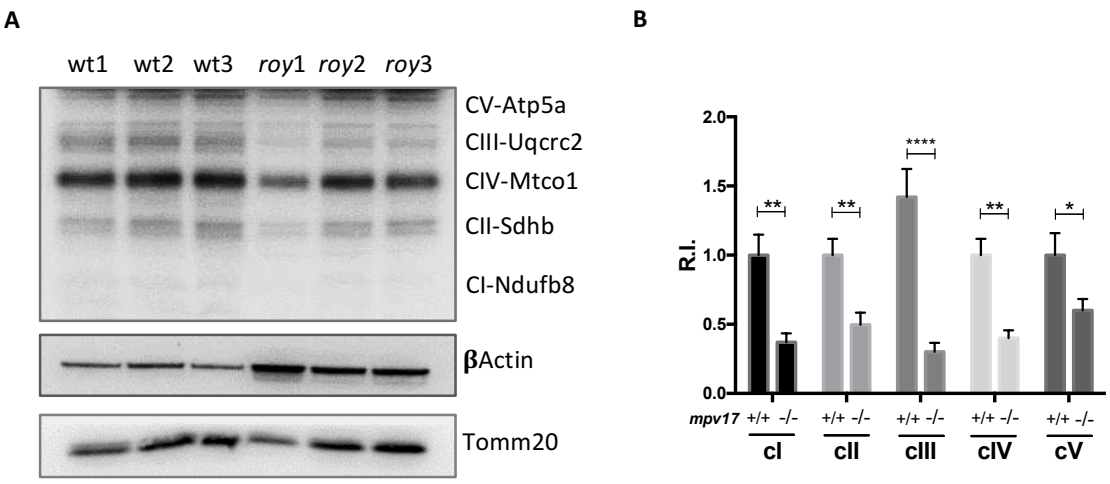

Figure 27. Western Blot analysis against different subunits of OXPHOS complexes (A), an antibody against βActin was used for standardization and relative quantification (B). Statistical analyses were performed by using Mann-Whitney unpaired non-parametric test. The statistical significance was evaluated by setting a confidence interval of 95%. The p values were set as follows: ****=p<0.0001; **=p<0.01; *=p<0.05.

Interestingly, our results showed a reduction of all RC in *roy* compared to wild-type and, in particular, the nuclear-encoded subunit Uqcrc2 of Ubiquinol–cytochrome c oxidoreductase (complex III) was found to be the most affected protein, with respect to the other OXPHOS complexes.

These data link the loss of mitochondrial ultrastructure and OXPHOS impairment to the reduction of RC protein subunits.

Moreover, since the decreased amount of RC subunits might be due to several defects, such as loss of mtDNA copy number, mitochondrial transcription or deficiencies of RC translation/assembly, we decided to test these different hypotheses.

2.4 *mpv17* homozygous mutants display mtDNA depletion at 10 dpf

Firstly, to understand whether mtDNA depletion caused the reduction of OXPHOS complexes, we quantified mtDNA copy number in *mpv17* homozygous mutants by

performing RT-qPCR analysis on DNA extracted from whole larvae at 3, 6 and 10 dpf (Fig.28).

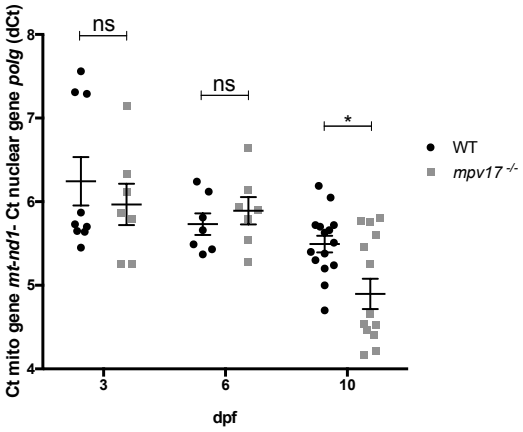

Figure 28. Relative quantification of mtDNA copy number in wild-type and mpv17 homozigous mutants. Mean dCt values were calculated as Ct of mt-nd1 (mitochondrially-encoded gene) minus Ct of polg1 (nuclear gene) and plotted with SEM. The statistical significance was evaluated by setting a confidence interval of 95%. The p values were set as follows: *=p<0.05; ns=not significant.

Interestingly, we found a significant reduction in mtDNA content in *mpv17*$^{-/-}$ larvae only from 10 dpf, when the morphological and respiratory mitochondrial phenotypes are already noticeable.

Since *MPV17*-related disease mostly shows hepatic and neurological manifestations and we found a strong mitochondrial phenotype in liver tissue, we measured mtDNA content in *roy* and wild type anterior trunk sections, in order to enrich the percentage of hepatic and neuronal cells in our samples (Fig.29).

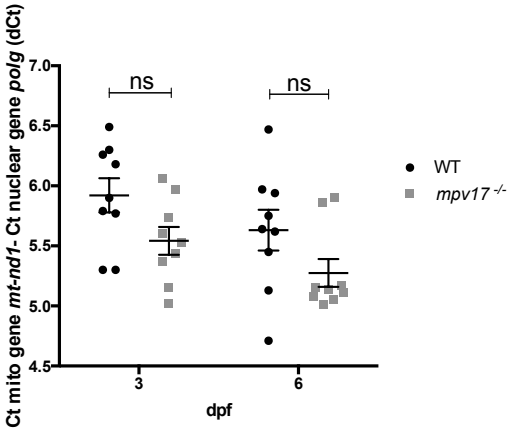

Figure 29. Relative quantification of mtDNA copy number in anterior trunk sections of wild-type and mpv17 homozigous mutants. Mean dCt values were calculated as Ct of mt-nd1 (mitochondrially-encoded gene) minus Ct of polg1 (nuclear gene) and plotted with SEM. The statistical significance was evaluated by setting a confidence interval of 95%. ns=not significant.

Also in this case, we did not observe any difference in mtDNA content comparing wild-type and *roy* sections at both 3 and 6 dpf.

It is well-known that OXPHOS complexes are composed of different subunits, that are respectively encoded by both nuclear and mitochondrial genes. An exception is represented by complex II, whose subunits are entirely encoded by nuclear genes (Schon, 2000). We therefore verified if the RC complex decrease we detected was due to a defect in mitochondrial and/or nuclear gene transcription of OXPHOS subunits. In particular, since OXPHOS complex III was found to be the most reduced complex, we decided to investigate expression levels of one nuclear-encoded subunit and one mitochondrial-encoded subunit of this complex (Fig.30).

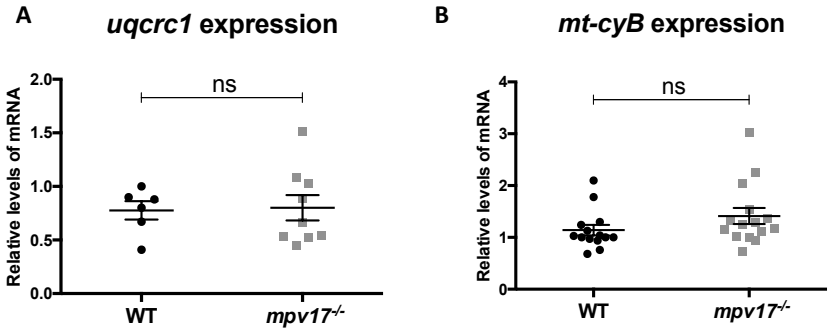

Figure 30. Real-time PCR quantification of mRNA transcripts from nuclear-encoded subunit (A) and mitochondrial-encoded subunit (B) of complex III. The statistical significance was evaluated by setting a confidence interval of 95%. ns= not significant.

Our results showed no significant defects in 6 dpf *roy* larvae in the nuclear and mitochondrial transcription of complex III subunits. From these analyses we can conclude that OXPHOS complex reduction in *roy orbison* is not caused by a defective transcription or mtDNA depletion but, rather, it is due to a potential impairment in assembly or translation leading to premature degradation.

2.5 Stress response and mitochondrial quality control are triggered in *roy orbison*

As we detected both morphological and functional alterations in *roy* mitochondria, we checked for a possible activation of stress response machinery. In fact, it is well-established that the molecular mechanisms of mitochondrial stress signaling pathways are quite complex and have dual functions in cell survival and death (Xue and Zhang, 2017). In particular, we focused on mitochondrial chaperon Grp75, a well-studied guardian against stress and apoptosis and a cytoprotective factor playing a central role in import/export of proteins (Kaul *et al.*, 2007). In particular, it is induced under different conditions, from glucose deprivation and oxidative injury to UVA radiations and drug administration (Liu *et al.*, 2005). By performing western blot analysis, we checked for Grp75 amount in *mpv17*$^{-/-}$ mutants at 6 dpf (Fig.31).

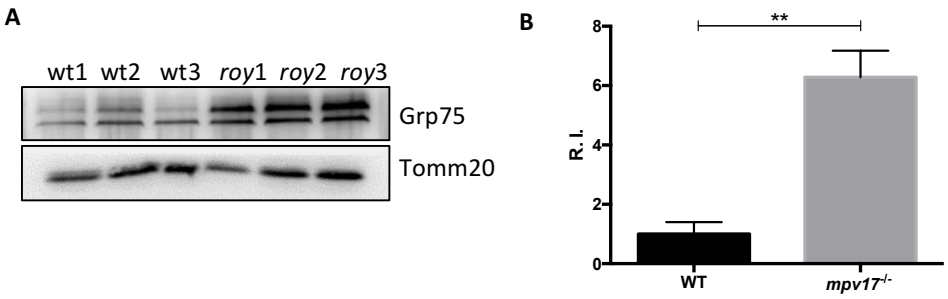

Figure 31. Representative western blot analysis of Grp75 protein from 6 dpf zebrafish larvae (A), and relative quantification, by using Tomm20 as normalizer (B). The statistical significance was evaluated by setting a confidence interval of 95%. **=p<0.01.

Notably, using an antibody against the mitochondrial outer membrane protein Tomm20 as normalizer, we found a significant increase of Grp75 amount in *mpv17* KO mutants compared to wild type. Hence, knowing that the *mitochondrial contact site and cristae organizing system* (MICOS) acts as a membrane-shaping and -connecting scaffold (Schorr and van der Laan, 2018) and has been proposed as a master regulator/integrator of IMM organization (Harner *et al.*, 2011), we tested whether the mitochondrial ultrastructure loss might activate the quality control system in mitochondria. MICOS is a huge complex composed of several proteins forming two subcomplexes that both contribute to membrane curvature stabilization and are connected via MIC19, which acts to regulate subcomplex distribution and cristae junction copy number (Friedman *et al.*, 2015).

In order to identify any change in gene expression as a response to cristae alterations we used RT-qPCR analysis to check at 6 dpf the transcriptional levels of several MICOS subunits: *mic60*, *mic13*, *mic19a* and *mic19b (*duplicated in the zebrafish genome) (Fig.32).

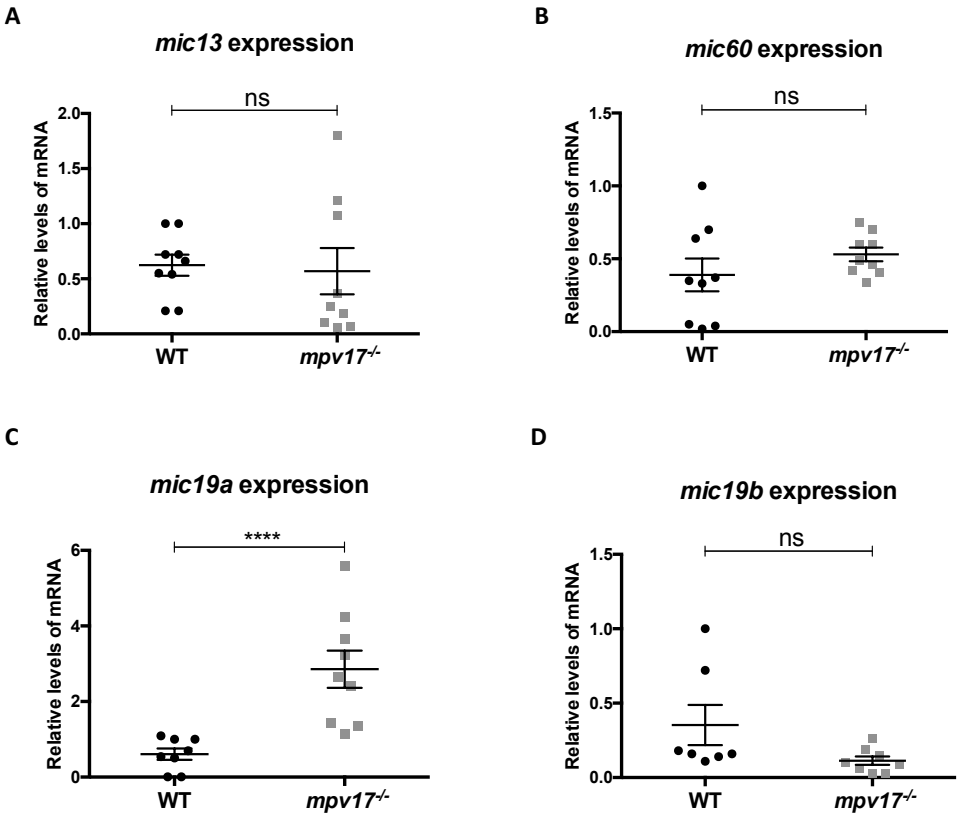

Figure 32. Real-time PCR quantification of mRNA transcripts from different MICOS subunits, respectively mic13 (A), mic60 (B), mic19a (C) and mic19b (D). The statistical significance was evaluated by setting a confidence interval of 95%. The p values were set as follows: ****=p<0.0001; ns=not significant.

Interestingly, when comparing wild-type to *roy orbison* larvae at 6 dpf we observed a transcriptional upregulation of *mic19a* in *roy*, while no differences were found in other MICOS transcripts.

3. Investigation of *mpv17* role

3.1 dNTP metabolism is linked to *roy* phenotype

Different studies in several *in vivo* models, based on common features of all the phenotypes caused by the loss of Mpv17, raised the hypothesis that the Mpv17 protein forms a channel in the inner mitochondrial membrane. The most recognised idea is that Mpv17 might be a channel allowing small molecules

(nucleotides in vertebrates, and intermediates of the TCA cycle in yeast) to pass (Löllgen and Weiher, 2014).

Considering previous studies suggesting a role for Mpv17 in mitochondrial dNTP metabolism (Dalla Rosa *et al.*, 2014, Krauss *et al.*, 2013) and taking advantage of the possibility to count iridophores, we tested in zebrafish the rescue of *roy* phenotype with different deoxynucleotides. In particular, we administrated a mixture of purine (dATP + dGTP); the pyrimidine precursor dUTP; and all these dNTPs together.

Thus, we evaluated the effect of these treatments at 3 dpf by performing birefringence analysis in the tail region and checking iridophore number (Fig.33).

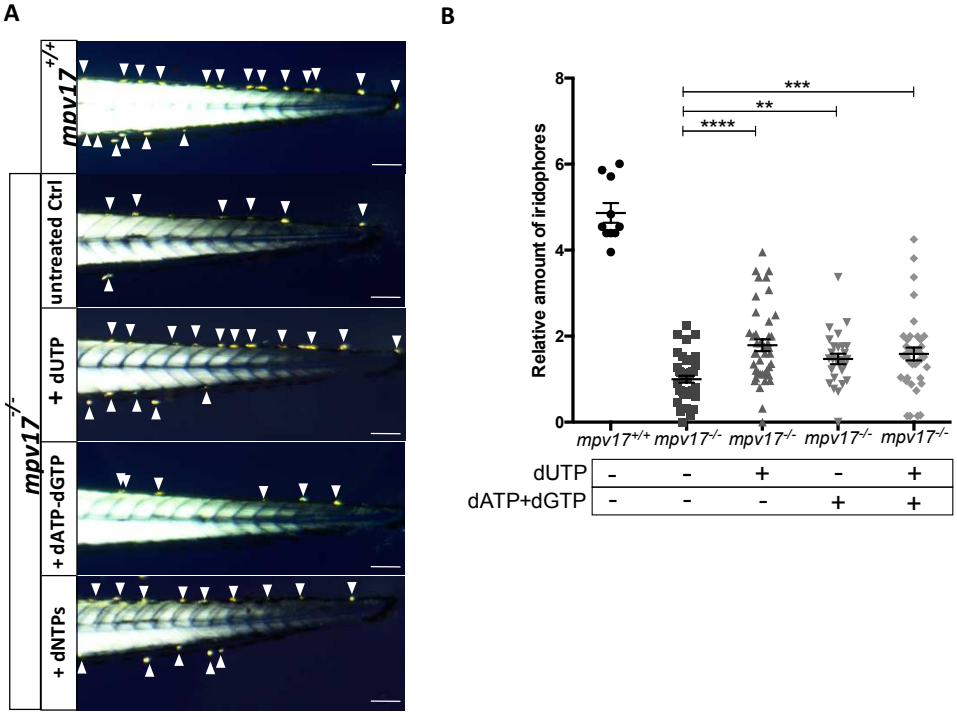

Figure 33. Administration of different mixtures of dNTPs (A) and relative quantification of relative amount of iridophores (B). Evaluation of iridophore number in the tail region, performed with the aid of two polarizing filters and based on the physical property of iridophores of being birefringent. The arrows point to iridophores. Bars, 100 µm. The statistical significance was evaluated by setting a confidence interval of 95%. The p values were set as follows: ****=p<0.0001; ***=p<0.001; **=p<0.01.

Interestingly, all dNTPs were able to increase iridophores number at 3 dpf and, in particular, dUTP administration showed the best effect in rescuing *roy* phenotype. These results suggest that Mpv17 loss could be linked to a defective nucleotide uptake and, specifically, that pyrimidine *de novo* synthesis may play an important role in iridophore development and differentiation.

3.2 Pyrimidine *de novo* synthesis is needed for iridophore development

To date, despite several works focusing on the identification of the biochemical role of MPV17 and its possible interactions with molecular pathways, its function remains poorly understood. For this reason, we performed a bioinformatics search on CORD platform to identify *MPV17* co-regulated genes (Fig.34).

Gene symbol	Description	# of experiments with MPV17	%concordant	Pearson Coef	Pearson p-val.
MPV17	MpV17 mitochondrial inner membrane protein [Source:HGNC Symbol;Acc:7224]	424			
MAGED1	melanoma antigen family D, 1 [Source:HGNC Symbol;Acc:6813]	176	88.6363636364	0.519030597265	1.28356075802e-30
GLB1	galactosidase, beta 1 [Source:HGNC Symbol;Acc:4298]	149	91.9463087248	0.510492925155	1.62691766014e-29
PGAM1	phosphoglycerate mutase 1 (brain) [Source:HGNC Symbol;Acc:8888]	172	87.7906976744	0.508691604107	2.75498214289e-29
CAD	carbamoyl-phosphate synthetase 2, aspartate transcarbamylase, and dihydroorotase [Source:HGNC Symbol;Acc:1424]	176	66.4772727273	0.503918624571	1.0957433225e-28
CNDP2	CNDP dipeptidase 2 (metallopeptidase M20 family) [Source:HGNC Symbol;Acc:24437]	175	84.0	0.503598549838	1.20110287317e-28
YWHAB	tyrosine 3-monooxygenase/tryptophan 5-monooxygenase activation protein, beta polypeptide [Source:HGNC Symbol;Acc:12849]	191	91.0994764398	0.49560445747	1.15309824315e-27
FUCA2	fucosidase, alpha-L- 2, plasma [Source:HGNC Symbol;Acc:4008]	150	92.6666666667	0.490884702241	4.26364953099e-27
FANCF	Fanconi anemia, complementation group F [Source:HGNC Symbol;Acc:3587]	100	89.0	0.486093506765	1.57520696874e-26
GBA	glucosidase, beta, acid [Source:HGNC Symbol;Acc:4177]	150	87.3333333333	0.485906687821	1.65686485517e-26
IDH3G	isocitrate dehydrogenase 3 (NAD+) gamma [Source:HGNC Symbol;Acc:5386]	139	90.6474820144	0.482629959765	4.0002403426e-26
HEXB	hexosaminidase B (beta polypeptide) [Source:HGNC Symbol;Acc:4879]	165	85.4545454545	0.477602077649	1.5187823520e-25
TBL1X	transducin (beta)-like 1X-linked [Source:HGNC Symbol;Acc:11585]	162	75.9259259259	0.468468216355	1.62131042545e-24
CD81	CD81 molecule [Source:HGNC Symbol;Acc:1701]	180	91.6666666667	0.467042697849	2.33127614232e-24
CTSD	cathepsin D [Source:HGNC Symbol;Acc:2529]	173	91.9075144509	0.463243470992	6.0864642081e-24
MCFD2	multiple coagulation factor deficiency 2 [Source:HGNC Symbol;Acc:18451]	197	89.3401015228	0.462693462979	5.9866595395 1e-24
CTSA	cathepsin A [Source:HGNC Symbol;Acc:9251]	114	90.350877193	0.461043508314	1.05517852598e-23
NME2	NME/NM23 nucleoside diphosphate kinase 2 [Source:HGNC Symbol;Acc:7850]	118	91.5254237288	0.455438251657	4.2111500268 2e-23
PPIB	peptidylprolyl isomerase B (cyclophilin B) [Source:HGNC Symbol;Acc:9255]	155	88.3870967742	0.454083035203	5.86228108546e-23
SLC38A10	solute carrier family 38, member 10 [Source:HGNC Symbol;Acc:28237]	123	95.1219512195	0.451567966058	1.0789274261e-22
SERPINH1	serpin peptidase inhibitor, clade H (heat shock protein 47), member 1, (collagen binding protein 1) [Source:HGNC Symbol;Acc:1546]	164	92.0731707317	0.446791749227	3.38908757451e-22
PPP1CA	protein phosphatase 1, catalytic subunit, alpha isozyme [Source:HGNC Symbol;Acc:9281]	125	87.2	0.44510334377	5.05752314664e-22
PLOD1	procollagen-lysine, 2-oxoglutarate 5-dioxygenase 1 [Source:HGNC Symbol;Acc:9081]	129	95.3488372093	0.441833289083	1.09120863073e-21
DBP	D site of albumin promoter (albumin D-box) binding protein [Source:HGNC Symbol;Acc:2697]	207	83.0917874396	0.440205260855	1.59527489813e-21
TSEN15	tRNA splicing endonuclease 15 homolog (S. cerevisiae) [Source:HGNC Symbol;Acc:16791]	60	96.6666666667	0.437965250784	2.68109323433e-21
GNS	glucosamine (N-acetyl)-6-sulfatase [Source:HGNC Symbol;Acc:4422]	190	80.5263157895	0.437951472304	2.68963699002e-21
CRTAP	cartilage associated protein [Source:HGNC Symbol;Acc:2379]	190	89.4736842105	0.43732697844	3.10637459412e-21
GLG1	golgi glycoprotein 1 [Source:HGNC Symbol;Acc:4316]	113	92.9203539823	0.433118049145	8.13825635339e-21
BACE1	beta-site APP-cleaving enzyme 1 [Source:HGNC Symbol;Acc:933]	198	89.898989899	0.429986746168	1.65175956867e-20
ALG5	asparagine-linked glycosylation 5, dolichyl-phosphate beta-glucosyltransferase homolog (S. cerevisiae) [Source:HGNC Symbol;Acc:20266]	116	82.7586206897	0.422905015426	7.97073966727e-20
NEU1	sialidase 1 (lysosomal sialidase) [Source:HGNC Symbol;Acc:7758]	150	82.6666666667	0.417421141773	2.62930547926e-19
ZFP1	zinc finger protein 1 homolog (mouse) [Source:HGNC Symbol;Acc:23328]	55	87.2727272727	0.416638528548	3.11202428193e-19
GSTO1	glutathione S-transferase omega 1 [Source:HGNC Symbol;Acc:13312]	176	86.3636363636	0.415561586846	3.92158880601e-19
TSEN34	tRNA splicing endonuclease 34 homolog (S. cerevisiae) [Source:HGNC Symbol;Acc:15506]	54	100.0	0.415357065956	4.09724242333e-19
HEXA	hexosaminidase A (alpha polypeptide) [Source:HGNC Symbol;Acc:4878]	140	84.2857142857	0.414082359695	5.38025750368e-19
GSS	glutathione synthetase [Source:HGNC Symbol;Acc:4624]	121	87.6033057851	0.413013651004	6.75470049517e-19

Figure 34. Bioinformatics search on CORD platform to identify MPV17 coregulated genes. The table shows a list of *MPV17* co-regulated genes based on the number of experiments, the percentage of concordance, Pearson coefficient and Pearson p-value.

Interestingly, we found that CAD enzyme, a trifunctional protein composed of Carbamoyl-phosphate synthetase 2, Aspartate transcarbamylase, and Dihydroorotase displays a 66.48% of concordant co-expression in 176 experiments, with a Pearson coefficient 0.504 and a p-value of 1.1x10-28, among

the highest scores of all *MPV17* co-regulated genes. CAD is known to be the rate-limiting enzyme for *de novo* biosynthesis of pyrimidine-based nucleotides and it catalyses the first three steps in *de novo* pyrimidine biosynthesis, in which ATP is used to convert glutamine and bicarbonate to dihydroorotic acid (DHOA) (Willer *et al.* 2005).

Most of the pyrimidine *de novo* synthesis takes place in cytosol, however, it requires a mitochondrial enzyme, Dihydroorotate dehydrogenase (Dhodh), needed for the conversion of DHOA into orotic acid (OA) (Fig.35).

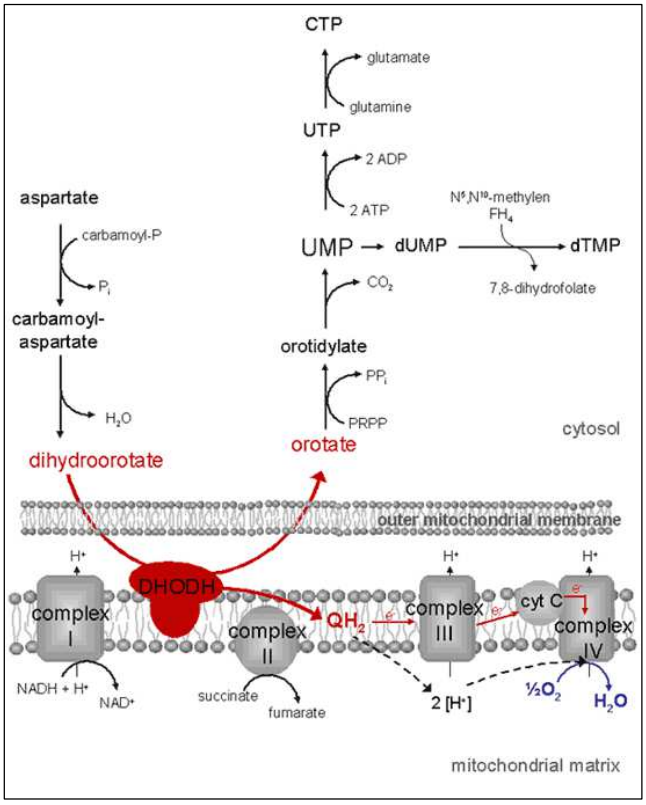

Figure 35. Schematic representation of pyrimidine de novo synthesis. dCTP and dTTP are synthesized from aspartate through the action of several cytosolic enzymes and the mitochondrial enzyme DHODH, that catalyzes the conversion of DHOA to OA in the fourth reaction step within pyrimidine synthesis. Thus, pyrimidine *de novo* synthesis is directly connected with the mitochondrial electron transport chain by DHODH, located inside mitochondrial cristae. (https://www.metabolic-database.com/html/dhodh.html#)

Thus, mitochondrial activity seems to be crucial for pyrimidine synthesis in order to ensure their availability for DNA replication. Most remarkable, evidences of a

possible connection between the pyrimidine *de novo* pathway and *mpv17* mutant phenotype were also coming from a previous work carried out by White *et al.* (2011). These authors reported that chemical inhibition of Dhodh by leflunomide is able to impair neural crest development by inducing the loss of both melanophores and iridophores in zebrafish. Leflunomide has multiple effects, including anti-proliferative, pro-apoptotic, anti-chemotherapeutic resistance, immunomodulatory, anti-inflammatory, anti-angiogenic and it represents a valuable compound to treat complex diseases, such as rheumatoid arthritis and cancer (Zhang *et al.*, 2018). Taking into account that melanophores are also impaired in *roy orbison* because of their strong interaction with iridophores, we wondered whether a mild Dhodh inhibition might selectively act on iridophore formation. Thus, we administrated leflunomide to 6 hpf wild-type embryos at lower concentrations, with respect to the work carried out by White and colleagues, and then evaluated the number of iridophores at 3 dpf (Fig.36).

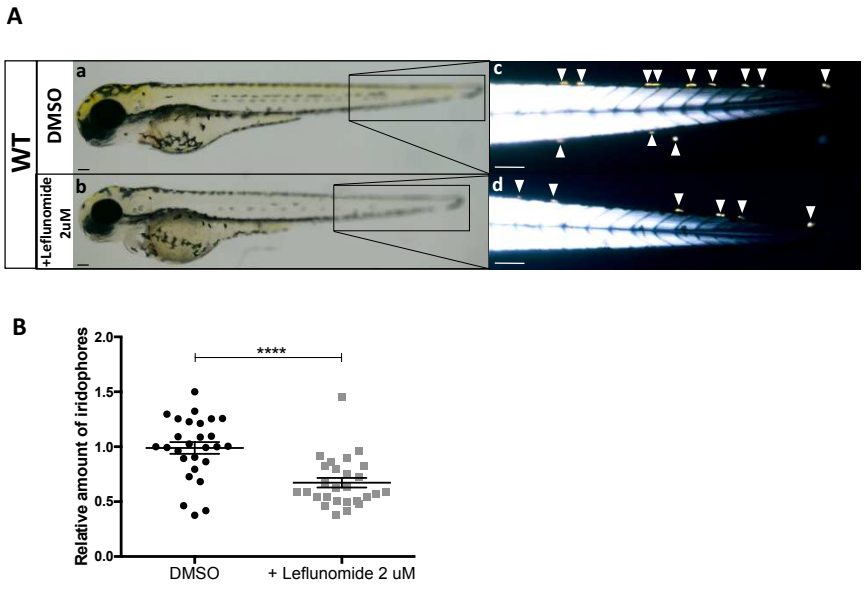

Figure 36. Leflunomide treatment on wild-type embryos from 6 to 72 hpf (A) and relative quantification of iridophore amount in the tail region (B). Bright-field picture of whole 3 dpf larva (a,b) and high-magnification image of tail iridophores by using birefringent lens (c,d). The arrows point to iridophores. Bars, 100 μm. The statistical significance was evaluated by setting a confidence interval of 95%. ****=p<0.0001.

Interestingly, our treatment specifically blocked iridophore differentiation and migration, while no other overt phenotypical effects could be observed. These results strongly suggest that Dhodh enzyme is needed for iridophore differentiation and that iridophores are the neural crest cells appearing most sensitive to a mild inhibition of this enzyme.

3.3 Orotic acid treatment restores iridophore formation and increases mtDNA copy number in *mpv17* null mutants

To support our hypothesis about a role of Dhodh in defective iridophore formation of *mpv17*$^{-/-}$ mutants, we tested whether administration of OA, the product of Dhodh reaction, might rescue *roy* phenotype.

OA is well-known as a precursor in biosynthesis of pyrimidines, in mammals it is released from DHODH and rapidly converted to uridine-5 -diphosphate (UDP), which is a precursor for production of cytosine- and thymine-based nucleotides and, ultimately, RNA and DNA synthesis (Willer *et al.* 2005). OA is mainly found in milk and dairy products, and it is converted to uridine for use in the pyrimidine salvage pathway predominantly in liver, kidney and erythrocytes. Early nutritional research identified orotic acid as "vitamin B13" and proposed it in therapies of metabolic syndromes (Löffler *et al*., 2016).

According to the protocol developed by Willer and colleagues (2005), OA was injected into the yolk sac of 20 hpf embryos. Then, we verify iridophore amount by performing birefringence analysis at 3 dpf (Fig.37).

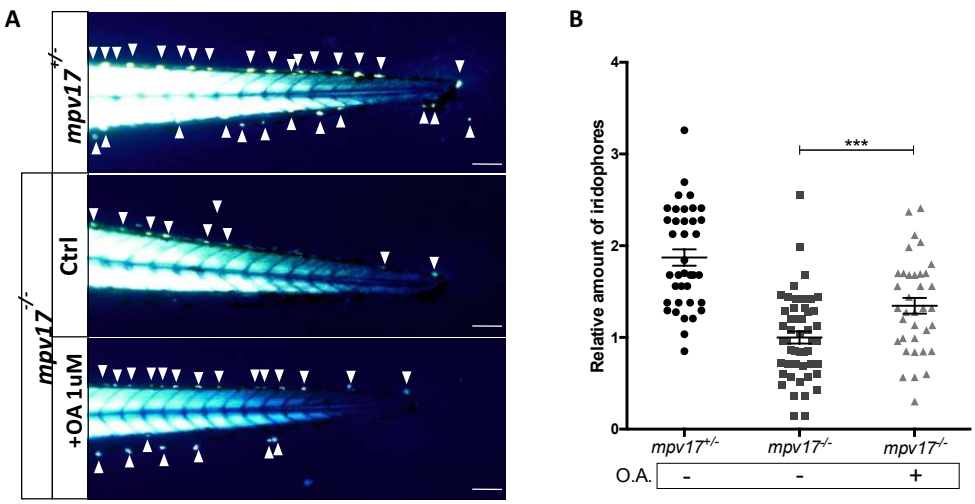

Figure 37. Administration of orotic acid and birefringence analysis at 3dpf in tail region (A). Relative quantification of iridophores amount (B). The arrows point to iridophores. Bars, 100 µm. The statistical significance was evaluated by setting a confidence interval of 95%. ***=p<0.001.

Interestingly, we observed a clear rescue of iridophores in *roy*, suggesting a link between *mpv17* mutant phenotype and pyrimidine precursors.

Since OA rescued iridophore phenotype, we assessed whether OA could also enhance mtDNA replication and/or stability, by performing RT-qPCR analysis on injected larvae and controls at 3 dpf (Fig.38).

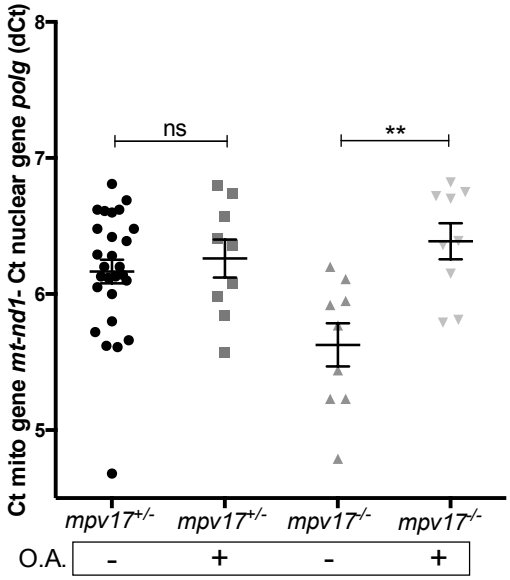

Figure 38. Relative quantification of mtDNA copy number in mpv17$^{+/-}$ and mpv17$^{-/-}$ 3dpf larvae. Mean dCt values were calculated as Ct of mt-nd1 (mitochondrially-encoded gene) minus Ct of polg1

(nuclear gene) and plotted with SEM. The statistical significance was evaluated by setting a confidence interval of 95%. The p values were set as follows: **=p<0.01; ns=not significant.

Although *mpv17* mutants displayed a constant, though non-significant, decrease in mtDNA copy number at 3 dpf. Interestingly, by evaluating the effect of OA administration at this selected time point, we observed that OA treatment specifically increased mtDNA copy number in *mpv17*$^{-/-}$ larvae, having no effect on heterozygotes.

These results highlight the importance of an efficient nucleotide uptake for the maintenance of mtDNA. In fact, mitochondrial DNA depletion syndromes have been previously associated with nine nuclear genes involved in the maintenance of mitochondrial dNTP pools, including Thymidine kinase 2 (*TK2*), Deoxyguanosine kinase (*DGOUK*), p53-dependent Ribonucleotide reductase subunit 2 (*RRM2B*) and Thymidine phosphorylase (*TYMP*) (Fasullo and Endres, 2015).

In addition, these data strongly suggest that, in absence of Mpv17, Dhodh enzyme does not properly convert DHOA and thus supply the cells with pyrimidines. To test this hypothesis, we assessed the effect of DHOA in *mpv17* mutants, by injecting *roy* embryos at 20 hpf with L-DHOA (Fig.39).

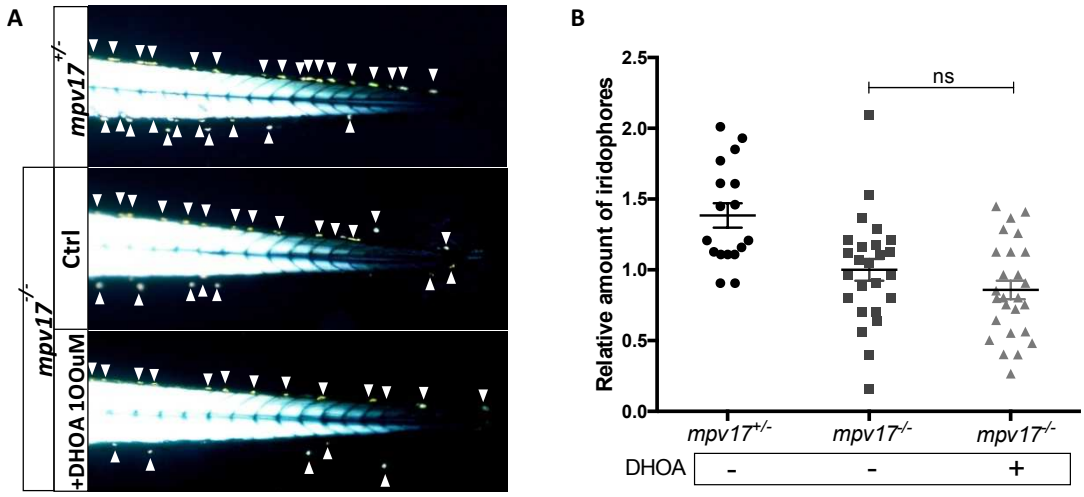

Figure 39. Administration of dihydroorotic acid and birefringence analysis at 3dpf in tail region (A). Relative quantification of iridophores amount (B). The arrows point to iridophores. Bars, 100 µm. The statistical significance was evaluated by setting a confidence interval of 95%. ns=not significant.

Notably, we were able to observe that DHOA treatment had no effect on iridophore amount, suggesting that it was unable to be converted into OA, stimulate pyrimidine synthesis and ameliorate *roy* phenotype.

Taken together, these results support the idea of a possible Dhodh impairment in *roy*, since this enzyme seemed to be not able to convert its substrate DHOA into OA and, thus, the administration of this precursor did not rescue *roy* phenotype.

In summary, our work validates *roy orbison* as a powerful model for investigating *MPV17*-related MDS and *MPV17* gene function, proposing a clear link between Mpv17, mitochondrial ultrastructure maintenance, OXPHOS functionality and pyrimidine *de novo* synthesis.

Discussion

Our work validates *roy orbison* as a model for investigating *mpv17* role and a powerful tool for developing new therapeutic strategies against *MPV17*-related MDS.

Firstly, we demonstrated *in vivo* that MPV17 can rescue the *roy* phenotype, supporting a conserved role between the two orthologues; this finding is also in agreement with complementation assays in the yeast *sym1Δ* model (Trott and Morano, 2004), that showed a functional link between SYM1 and mammalian MPV17 homologues.

Interestingly, by performing different techniques, we could observe an increased expression of *mpv17l2* in *mpv17* null mutants. Moreover, overexpression of Mpv17L2 is able to rescue the *roy* chromatophore phenotype. These two findings support the idea of overlapping metabolic functions for Mpv17 and Mpv17L2, at least in zebrafish. This contrasts, evolutionary, with previous works carried out in human cellular models, suggesting different roles for MPV17, claimed to be involved in purine synthesis (Dalla Rosa *et al.* 2016), and MPV17L2, suggested to play a role in mitochondrial ribosome assembly (Dalla Rosa *et al.* 2014). However, we did not observe any significant effect of *mpv17-like2* mRNA injection on mtDNA stability. A possible explanation is the lack of significant mtDNA replication, unnecessary at early stages of development (Artuso *et al.*, 2012), thus hampering the evaluation on the role of *mpv17-like2* at these time points. Because of that, stable lines overexpressing *mpv17-like2* in *roy* mutant background may be useful tools for following its effect on *roy* phenotype at later stages of development. Nevertheless, our data reveal new potential scenarios for *MPV17-like2* role, which

might be further investigated as a potential novel target in *MPV17*-related disease therapy. Taking into account that no zebrafish mutant for *mpv17-like2* were available, we decided to generate a mutant line by performing CRISPR/Cas technology, largely applied to zebrafish model. We therefore obtained and validated a *mpv17l2* Δ7 mutant line, showing no macroscopical phenotype in homozygous state we will further characterize. Considering *mpv17l2* Δ7 mutant phenotype, it therefore has to be said that no pathogenic variants have been identified in *MPV17-like2* gene so far, thus supporting the idea that the human orthologue may also play a replaceable role.

In the last two decades, different *MPV17*-related MDS models have been developed, all showing phenotypes which are only partially representative of human clinical features. While the *Mpv17* KO mouse strain mainly shows glomerulosclerosis and inner ear defects (Löllgen and Weiher, 2014), the zebrafish *roy* phenotype is mostly characterized by a specific lack of iridophores and a progressive loss of melanophores, both cell lineages derived from neural crest. This phenotype matches with clearly recognizable as neurocristopathy features such as premature graying of mouse Mpv17 KO (Viscomi *et al.*, 2008) and retinopathy and progressive demyelinating peripheral neuropathy, found in 10% and 38% of *MPV17* patients, respectively (El Hattab *et al.*, 2017). In addition, in this work we demonstrate that zebrafish *mpv17* KO larvae also display a severe mitochondrial phenotype, characterized by mitochondrial cristae disappearance in liver hepatocytes; impairment of OXPHOS functionality; reduction of RC protein amount; mtDNA depletion and activation of mitochondrial stress response. Particularly, mitochondrial ultrastructure alterations were previously found in *Mpv17* KO mouse liver (Viscomi *et al.*, 2008) and in yeast *sym1*Δ model (Dallabona

et al., 2009). Interestingly, Dallabona and colleagues suggested Sym1 as primarily involved in mitochondrial ultrastructure maintenance, taking into account that the loss of cristae architecture affects mtDNA stability and supercomplex arrangement within IMM (Stuart, 2008). Our findings strongly support this hypothesis since we were able to observe a significant reduction of mtDNA copy number only at 10 dpf, while mitochondrial ultrastructure and RC amount were shown to be already impaired at 6 dpf.

Moreover, a tissue-specific dysfunction of OXPHOS complexes was frequently found in patients affected by different mutations in the *MPV17* gene (Spinazzola *et al.*, 2006; Uusimaa *et al.*, 2014; El Hattab *et al.*, 2018). All considered, our results prove that the *mpv17* null mutant perfectly resembles the human mitochondrial phenotype, thus suggesting *roy orbison* as a good model for *MPV17*-related MDS. Additionally, the overproduction of Grp75 and the overexpression of *mic19a* that we found in *roy* highlight the importance of *mpv17* in preserving mitochondrial homeostasis, suggesting that, in the absence of Mpv17, protective mechanisms act against oxidative stress and loss of mitochondrial morphology. Interestingly, the *grp75* yeast orthologous gene, *SSC1*, was also found upregulated at the transcriptional level in the yeast *mpv17*-orthologue mutant *sym1Δ* (Trott and Morano, 2004). Moreover, GRP75 was previously suggested to inhibit ROS accumulation, displaying a cytoprotective effect (Liu *et al.*, 2005) and enhanced ROS levels were previously reported in mice and cell lines depleted of Mpv17 (Wagner *et al.*, 2001; Shvetsova *et al.*, 2017).

Despite *MPV17* was discovered about thirty years ago, its function remains unknown and the leading hypothesis is that MPV17 may represent an inner

mitochondrial membrane protein involved in nucleotide supply for mtDNA synthesis (Löllgen and Weiher, 2014; Krauss *et al.*, 2013).

As for other MDS, *MPV17* mutations might impair deoxyribonucleotide metabolism, leading to limited dNTP availability and subsequent mtDNA depletion. To date, dNTP administration is a therapeutic strategy for treatment of MNGIE mtDNA depletion syndrome (Camara *et al.*, 2013) and it was previously reported that supplementation with different amino acids, all nucleotide precursors, partially restored aerobic oxidative growth of the yeast *sym1*Δ strain (Dallabona *et al.*, 2009). Coherently, we found that deoxyribonucleotide administration strongly increased iridophore number in *mpv17*$^{-/-}$ larvae and, in particular, since dUTP showed the best effect, we focused on pyrimidine *de novo* synthesis. Interestingly, we found, by performing a bioinformatics analysis, that *MPV17* and *CAD*, a cytosolic enzyme involved in pyrimidine production, are highly co-regulated. Moreover, considering the well-established link between Dhodh mediated-mitochondrial step of pyrimidine production and neural crest cell formation (White *et al.*, 2011), we observed that a mild inhibition of Dhodh enzyme specifically impaired iridophore development and that administration of orotic acid, but not dihydroorotic acid, significantly rescued the *roy* phenotype. Taken together our results indicate an ineffective pyrimidine supply and an impairment of Dhodh in *mpv17*$^{-/-}$ null mutants, which may be primary due to either the disruption of mitochondrial cristae, in which it is located, or to a possible interaction between this enzyme and Mpv17.

Hence, the specific effect of orotic acid in increasing mtDNA content in *roy*, the great availability of this nutrient in dairy products, and its current use as food

supplement open up new opportunities in the treatment of *MPV17*-related MDS, to date a disease with poor prognosis and not yet available cure.

Note that this work would have not been possible without the support from CARIPARO foundation and the generosity of Telethon and its donors.

References

Antonenkov V.D., Isomursu A., Mennerich D., Vapola M.H., Weiher H., Kietzmann T., Hiltunen J.K., 2015. **The Human Mitochondrial DNA Depletion Syndrome Gene *MPV17* Encodes a Non-selective Channel That Modulates Membrane Potential.** J. Biol. Chem., 290, 13840-13861. https://doi.org/10.1074/jbc.M114.608083.

Artuso, L., Romano, A., Verri, T., Domenichini, A., Argenton, F., Santorelli, F.M., Petruzzella, V., 2012. **Mitochondrial DNA metabolism in early development of zebrafish (*Danio rerio*)**. Biochim. Biophys. Acta (BBA) - Bioenergetics, 1817, 1002-1011. https://doi.org/10.1016/j.bbabio.2012.03.019.

Cade L., Reyon D., Hwang W.Y., Tsai S.Q., Patel S., Khayter C., Joung J.K., Sander J.D., Peterson R.T., Yeh J.R., 2012. **Highly efficient generation of heritable zebrafish gene mutations using homo- and heterodimeric TALENs.** Nucleic Acids Res., 40(16):8001-10. https://doi.org/10.1093/nar/gks518.

Calvo, S.E., Clauser, K.R., Mootha, V.K., 2016. **MitoCarta2.0: an updated inventory of mammalian mitochondrial proteins.** Nucleic Acids Res., 44, D1251–D1257. https://doi.org/10.1093/nar/gkv1003.

Cámara, Y., González-Vioque, E., Scarpelli, M., Torres-Torronteras, J., Caballero, A., Hirano, M., Martí, R., 2014. **Administration of deoxyribonucleosides or inhibition of their catabolism as a pharmacological approach for mitochondrial DNA depletion syndrome.** Hum. Mol. Genet., 23, 2459–2467. https://doi.org/10.1093/hmg/ddt641.

Chang N., Sun C., Gao L., Zhu D., Xu X., Zhu X., Xiong J.W., Xi J.J., 2013. **Genome editing with RNA-guided Cas9 nuclease in zebrafish embryos.** Cell Res. 2013 Apr;23(4):465-72. https://doi.org/10.1038/cr.2013.45.

Chinnery, P.F., Hudson, G., 2013. **Mitochondrial genetics.** Br. Med. Bull., 106, 135–159. https://doi.org/10.1093/bmb/ldt017.

Dahm R., Geisler R., 2006. **Learning from small fry: the zebrafish as a genetic model organism for aquaculture fish species.** Mar. Biotechnol., 8, 329-345. https://doi.org/10.1007/s10126-006-5139-0.

Dallabona, C., Marsano, R.M., Arzuffi, P., Ghezzi, D., Mancini, P., Zeviani, M., Ferrero, I., Donnini, C., 2010. **Sym1, the yeast ortholog of the MPV17 human disease protein, is a stress-induced bioenergetic and morphogenetic mitochondrial modulator.** Human. Mol. Genet., 19, 1098–1107. https://doi.org/10.1093/hmg/ddp581.

Dalla Rosa, I., Cámara, Y., Durigon, R., Moss, C.F., Vidoni, S., Akman, G., Hunt, L., Johnson, M.A., Grocott, S., Wang, L., Thorburn, D.R., Hirano, M., Poulton J., Taylor, R.W., Elgar, G., Martí, R., Voshol, P., Holt, I.J., Spinazzola A., 2016. **MPV17 Loss Causes Deoxynucleotide Insufficiency and Slow DNA Replication in Mitochondria.** PLoS Genet. 12(1): e1005779. https://doi.org/10.1371/journal.pgen.1005779.

Dalla Rosa, I., Durigon, R., Pearce, S.F., Rorbach, J., Hirst, E.M.A., Vidoni, S., Reyes, A., Brea-Calvo, G., Minczuk, M., Woellhaf, M.W., Herrmann, J.M., Huynen, M.A., Holt, I.J., Spinazzola, A., 2014. **MPV17L2 is required for ribosome assembly in mitochondria**. Nucleic Acids Res., 42, 8500–8515 https://doi.org/10.1093/nar/gku513.

D'Agati, G., Beltre, R., Sessa, A., Burger, A., Zhou, Y., Mosimann, C., White, R.M., 2017. **A defect in the mitochondrial protein Mpv17 underlies the transparent casper zebrafish.** Dev. Biol., 430, 11-17. https://doi.org/10.1016/j.ydbio.2017.07.017.

El-Hattab A.W., Li F.Y., Schmitt E., Zhang S., Craigen W.J., Wong L.J., 2010. **MPV17-associated hepatocerebral mitochondrial DNA depletion syndrome: new patients and novel mutations.** Mol Genet Metab., 99(3):300-8. https://doi.org/10.1016/j.ymgme.2009.10.003.

El-Hattab A.W., Scaglia F., 2013. **Mitochondrial DNA depletion syndromes: review and updates of genetic basis, manifestations, and therapeutic options.** Neurotherapeutics, 10, 186-198. https://doi.org/10.1007/s13311-013-0177-6.

El-Hattab, A.W., Wang, J., Dai, H., Almannai, M., Staufner, C., Alfadhel, M., Gambello, M.J., Prasun, P., Raza, S., Lyons, H.J., Afqi, M., Saleh, M.A.M., Faqeih, E.A., Alzaidan, H.I., Alshenqiti, A., Flore, L.A., Hertecant, J., Sacharow, S., Barbouth, D.S, Murayama, K., Shah, A.A., Lin, H.C., Wong, L.J.C., 2018. **MPV17-related mitochondrial DNA maintenance defect: New cases and review of clinical, biochemical, and molecular aspects.** Hum. Mut., 39, 461–470. https://doi.org/10.1002/humu.23387.

Fasullo M., Endres L., 2015. **Nucleotide salvage deficiencies, DNA damage and neurodegeneration.** Int J Mol Sci, 16(5):9431-49. https://doi.org/10.3390/ijms16059431.

Friedman J.R., Mourier A., Yamada J., McCaffery J.M., Nunnari J., 2015. **MICOS coordinates with respiratory complexes and lipids to establish mitochondrial inner membrane architecture.** Elife, 28;4. https://doi.org/10.7554/eLife.07739.

Frohnhöfer, H.G., Krauss, J., Maischein, H.M., Nüsslein-Volhard, C., 2013. **Iridophores and their interactions with other chromatophores are required for stripe formation in zebrafish.** Development, 140, 2997-3007. https://doi.org/10.1242/dev.096719.

Gunbin K., Peshkin L., Popadin K., Annis S., Ackermann R.R., Khrapko K., 2017. **Integration of mtDNA pseudogenes into the nuclear genome coincides with speciation of the human genus. A hypothesis.** Mitochondrion, 34:20-23. https://doi.org/10.1016/j.mito.2016.12.001.

Haft D.H., Selengut J., Mongodin E.F., Nelson K.E., 2005. **A guild of 45 CRISPR-associated (Cas) protein families and multiple CRISPR/Cas subtypes exist in prokaryotic genomes.** PLoS Comput Biol.,1(6):e60. https://doi.org/10.1371/journal.pcbi.0010060.

Harner M., Körner C., Walther D., Mokranjac D., Kaesmacher J., Welsch U., Griffith J., Mann M., Reggiori F., Neupert W., 2011. **The mitochondrial contact site complex, a determinant of mitochondrial architecture.** EMBO J., 30(21):4356-70. https://doi.org/10.1038/emboj.2011.379.

Higdon, C.W., Mitra, R.D., Johnson, S.L., 2013. **Gene expression analysis of zebrafish melanocytes, iridophores, and retinal pigmented epithelium reveals indicators of biological function and developmental origin.** PLoS One, 8(7):e67801. https://doi.org/10.1371/journal.pone.0067801.ù.

Howe K., Clark M.D., Torroja C.F., Torrance J., Berthelot C., Muffato M., Collins J.E., Humphray S., McLaren K., Matthews L., McLaren S. *et al.*, 2013. **The zebrafish reference genome sequence and its relationship to the human genome.** Nature 496, 498-503. https://doi.org/10.1038/nature12111.

Hwang W.Y., Fu Y., Reyon D., Maeder M.L., Kaini P., Sander J.D., Joung J.K., Peterson R.T., Yeh J.R., 2013. **Heritable and precise zebrafish genome editing using a CRISPR-Cas system.** PLoS One, 9;8(7):e68708. https://doi.org/10.1371/journal.pone.0068708.

Iida R., Yasuda T., Tsubota E., Takatsuka H., Masuyama M., Matsuki T., Kishi K., 2003 **M-LP, Mpv17-like protein, has a peroxisomal membrane targeting signal comprising a transmembrane domain and a positively charged loop and up-regulates expression of the manganese superoxide dismutase gene.** J Biol Chem., 278(8):6301-6. https://doi.org/10.1074/jbc.M210886200.

Jao L.E., Wente S.R., Chen W., 2013. **Efficient multiplex biallelic zebrafish genome editing using a CRISPR nuclease system.** Proc Natl Acad Sci U S A., 110(34):13904-9. https://doi.org/10.1073/pnas.1308335110.

Liu, Y., Liu, W., Song, X.D., Zuo, J., 2005. **Effect of GRP75/mthsp70/ PBP74/mortalin overexpression on intracellular ATP level, mitochondrial membrane potential and ROS accumulation following glucose deprivation in PC 12 cells.** Mol. Cell Biochem. 268, 45–51.

Karadimas, C.L., Vu, T.H., Holve, S.A., Chronopoulou, P., Quinzii, C., Johnsen, S.D., Kurth, J., Eggers, E., Palenzuela, L., Tanji, K., Bonilla, E., De Vivo, D.C., DiMauro, S., Hirano, M., 2006. **Navajo Neurohepatopathy Is Caused by a Mutation in the MPV17 Gene.** Am. J. Hum. Genet., 79, 544-548. https://doi.org/10.1086/506913.

Kaul, S.C., Deocaris, C.C., Wadhwa, R., 2007. **Three faces of mortalin: A housekeeper, guardian and killer.** Exp. Gerontol., 42, 263-274. https://doi.org/10.1016/j.exger.2006.10.020.

Krick, S., Shi, S., Ju, W., Faul, C., Tsai, S., Mundel, P., Böttinger, E.P., 2008. **Mpv17l protects against mitochondrial oxidative stress and apoptosis by activation of Omi/HtrA2 protease.** PNAS 105, 14106-14111. https://doi.org/10.1073/pnas.0801146105.

Krauss J., Astrinidis P., Frohnhöfer H.G., Walderich B., Nüsslein-Volhard C., 2013. **transparent, a gene affecting stripe formation in Zebrafish, encodes the mitochondrial protein Mpv17 that is required for iridophore survival.** Biol. Open., 2, 703-710. https://doi.org/10.1242/bio.20135132.

Labun K., Montague T.G., Gagnon J.A., Thyme S.B., Valen E., 2016. **CHOPCHOP v2: a web tool for the next generation of CRISPR genome engineering.** Nucleic Acids Res. 2016 Jul 8;44(W1):W272-6. https://doi.org/10.1093/nar/gkw398.

Liu Y., Liu W., Song X.D., Zuo J., 2005. **Effect of GRP75/mthsp70/PBP74/mortalin overexpression on intracellular ATP level, mitochondrial membrane potential and ROS accumulation following glucose deprivation in PC12 cells.** Mol Cell Biochem., 268(1-2):45-51.

Löffler M., Carrey E.A., Zameitat E., 2016. **Orotate (orotic acid): An essential and versatile molecule.** Nucleosides Nucleotides Nucleic Acids. 2016 Dec;35(10-12):566-577. https://doi.org/10.1080/15257770.2016.1147580.

Löllgen, S., Weiher, H., 2014. **The role of the Mpv17 protein mutations of which cause mitochondrial DNA depletion syndrome (MDDS): lessons from homologs in different species.** J. Biol. Chem., 396, 13-25. https://doi.org/10.1515/hsz-2014-0198.

Maharjan, S., Oku, M., Tsuda, M., Hoseki, J., Sakai, Y., 2014. **Mitochondrial impairment triggers cytosolic oxidative stress and cell death following proteasome inhibition.** Sci. Rep., 4, 5896. https://doi.org/10.1038/srep05896.

Makarova K.S., Wolf Y.I., Alkhnbashi O.S., Costa F., Shah S.A., Saunders S.J., Barrangou R., Brouns S.J., Charpentier E., Haft D.H., Horvath P., Moineau S., Mojica F.J., Terns R.M., Terns M.P., White M.F., Yakunin A.F., Garrett R.A., van der Oost J., Backofen R., Koonin E.V., 2015. **An updated evolutionary classification of CRISPR-Cas systems.** Nat Rev Microbiol., 13(11):722-36. https://doi.org/10.1038/nrmicro3569.

Marraffini L.A., Sontheimer E.J., 2010. **CRISPR interference: RNA-directed adaptive immunity in bacteria and archaea.** Nat Rev Genet., 11(3):181-90. https://doi.org/10.1038/nrg2749.

Moraes C.T., Shanske S., Tritschler H.J., Aprille J.R., Andreetta F., Bonilla E., Schon E.A., DiMauro S., 1991. **mtDNA depletion with variable tissue expression: a novel genetic abnormality in mitochondrial diseases.** Am J Hum Genet, 48(3):492-501.

Nogueira, C., Almeida, L.S., Nesti, C., Pezzini, I., Videira, A., Vilarinho, L. and Santorelli, F.M., 2014. **Syndromes associated with mitochondrial DNA depletion.** Ital. J. Pediatr., 40, 34. https://doi.org/10.1186/1824-7288-40-34.

Parikh S., Karaa A., Goldstein A, Ng Y.S., Gorman G., Feigenbaum A., Christodoulou J., Haas R., Tarnopolsky M., Cohen B.K., Dimmock D., Feyma T., Koenig M.K., Mundy H., Niyazov D., Saneto R.P., Wainwright M.S., Wusthoff C., McFarland R., Scaglia F., 2016. **Solid organ transplantation in primary mitochondrial disease: Proceed with caution.** Mol Genet Metab., 118(3):178-84. https://doi.org/10.1016/j.ymgme.2016.04.009.

Reinhold R., Krüger V., Meinecke M., Schulz C., Schmidt B., Grunau S.D., Guiard B., Wiedemann N., van der Laan M., Wagner R., Rehling P., Dudek J., 2012. **The channel-forming Sym1 protein is transported by the TIM23 complex in a presequence-independent manner.** Mol. Cell. Biol. 32, 5009-5021. https://doi.org/10.1128/MCB.00843-12.

Rokka A., Antonenkov V.D., Soininen R., Immonen H.L., Pirilä P.L., Bergmann U., Sormunen R.T., Weckström M., Benz R., Hiltunen J.K., 2009. **Pxmp2 is a channel-forming protein in Mammalian peroxisomal membrane.** PLoS ONE, 4(4):e5090. https://doi.org/10.1371/journal.pone.0005090.

Rossi, A., Kontarakis, Z., Gerri, C., Nolte, H., Hölper, S., Krüger, M., Stainier D.Y.R., 2015. **Genetic compensation induced by deleterious mutations but not gene knockdowns.** Nature, 524, 230–233. https://doi.org/10.1038/nature14580.

Sarzi E., Bourdon A., Chrétien D., Zarhrate M., Corcos J., Slama A., Cormier-Daire V., de Lonlay P., Munnich A., Rötig A., 2007. **Mitochondrial DNA depletion is a**

prevalent cause of multiple respiratory chain deficiency in childhood. J. Pediatr, 150, 531-534. https://doi.org/10.1016/j.jpeds.2007.01.044.

Schenkel J., Zwacka R.M., Rutenberg C., Reuter A., Waldherr R., Weiher H., 1995. **Functional rescue of the glomerulosclerosis phenotype in Mpv17 mice by transgenesis with the human Mpv17 homologue.** Kidney Int., 48(1):80-4. https://doi.org/10.1038/ki.1995.270.

Schon E.A., 2000. Mitochondrial genetics and disease. Trends Biochem Sci., 25(11):555-60. https://doi.org/10.1016/S0968-0004(00)01688-1.

Schorr, S., van der Laan, M., 2018. **Integrative functions of the mitochondrial contact site and cristae organizing system.** Semin. Cell. Dev. Biol., 76, 191-200. https://doi.org/10.1016/j.semcdb.2017.09.021.

Shvetsova, A.N., Mennerich, D., Kerätär, J.M., Kalervo Hiltunen, J., Kietzmann, T., 2017. **Non-electron transfer chain mitochondrial defects differently regulate HIF-1α degradation and transcription.** Redox Biol., 12, 1052-1061. https://doi.org/10.1016/j.redox.2017.05.003.

Spinazzola A., Massa V., Hirano M., Zeviani M., 2008. **Lack of founder effect for an identical mtDNA depletion syndrome (MDS)-associated MPV17 mutation shared by Navajos and Italians.** Neuromuscul Disord. 18(4):315-8. https://doi.org/10.1016/j.nmd.2007.12.007.

Spinazzola, A., Viscomi, C., Fernandez-Vizarra, E., Carrara, F., D'Adamo, P., Calvo, S., Marsano, R.M., Donnini, C., Weiher, H., Strisciuglio, P., Parini, R., Sarzi, E., Chan, A., DiMauro, S., Rötig, A., Gasparini, P., Ferrero, I., Mootha, V.K., Tiranti, V., Zeviani, M., 2006. **MPV17 encodes an inner mitochondrial membrane protein and is mutated in infantile hepatic mitochondrial DNA depletion.** Nat. Genet. 38, 570–575. https://doi.org/10.1038/ng1765.

Stoldt S., Wenzel D., Kehrein K., Riedel D., Ott M., Jakobs S., 2018. **Spatial orchestration of mitochondrial translation and OXPHOS complex assembly.** Nat Cell Biol., 20(5):528-534. https://doi.org/10.1038/s41556-018-0090-7.

Stuart, R.A., 2008. **Supercomplex organization of the oxidative phosphorylation enzymes in yeast mitochondria.** J. Bioenerg. Biomembr., 40, 411. https://doi.org/10.1007/s10863-008-9168-4.

Suomalainen A., Isohanni P., 2010. **Mitochondrial DNA depletion syndromes--many genes, common mechanisms.** Neuromuscul Disord, 20(7):429-37. https://doi.org/10.1016/j.nmd.2010.03.017.

Trott A., Morano K.A., 2004. **SYM1 is the stress-induced Saccharomyces cerevisiae ortholog of the mammalian kidney disease gene Mpv17 and is required for ethanol metabolism and tolerance during heat shock.** Eukaryot. Cell., 3, 620-631. https://doi.org/10.1128/EC.3.3.620-631.2004.

Uusimaa, J., Evans, J., Smith, C., Butterworth, A., Craig, K., Ashley, N., Liao, C., Carver, J., Diot, A., Macleod, L., Hargreaves, I., Al-Hussaini, A., Faqeih, E., Asery, A., Al Balwi, M., Eyaid, E., Al-Sunaid, A., Kelly, D., van Mourik, I., Ball, S., Jarvis, J., Mulay, A., Hadzic, N., Samyn. M., Baker, A., Rahman, S., Stewart, H., Morris, A.A.M., Seller, A., Fratter, C., Taylor R.W., Poulton, J., 2014. **Clinical, biochemical, cellular and molecular characterization of mitochondrial DNA depletion syndrome due to novel mutations in the MPV17 gene.** Eur. J. Hum. Genet., 22, 184–191. https://doi.org/10.1038/ejhg.2013.112.

van der Oost J., Westra E.R., Jackson R.N., Wiedenheft B., 2014. **Unravelling the structural and mechanistic basis of CRISPR-Cas systems.** Nat Rev Microbiol., 12(7):479-92. https://doi.org/10.1038/nrmicro3279.

Varshney G.K., Sood R., Burgess S.M., 2015. **Understanding and Editing the Zebrafish Genome.** Adv Genet, 92:1-52. https://doi.org/10.1016/bs.adgen.2015.09.002.

Viscomi, C., Spinazzola, A., Maggioni, M., Fernandez-Vizarra, E., Massa, V., Pagano, C., Vettor, R., Mora, M., Zeviani, M., 2009. **Early-onset liver mtDNA depletion and late-onset proteinuric nephropathy in Mpv17 knockout mice.** Hum. Mol. Genet. 18, 12–26. https://dx.doi.org/10.1093/hmg/ddn309.

Wagner, G., Stettmaier, K., Bors, W., 2005. **Enhanced Gamma-Glutamyl Transpeptidase Expression and Superoxide Production in Mpv17$^{-/-}$ Glomerulosclerosis Mice.** J. Biol. Chem., 382, 1019-1025. https://doi.org/10.1515/BC.2001.128.

Weiher, H., Noda, T., Gray, D.A., Sharpe, A.H. and Jaenisch, R., 1990. **Transgenic mouse model of kidney disease: insertional inactivation of ubiquitously expressed gene leads to nephrotic syndrome.** Cell, 62,425 – 434.

White, R.M., Cech, J., Ratanasirintrawoot, S., Lin, C.Y., Rahl, P.B., Burke, C.J., Langdon, E., Tomlinson, M.L., Mosher, J., Kaufman, C., Chen, F., Long, H.K., Kramer, M., Datta, S., Neuberg, D., Granter, S., Young, R.A., Morrison, S., Wheeler, G.N., Zon, L.I., 2011. **DHODH modulates transcriptional elongation in the neural crest and melanoma.** Nature, 471, 518–522. https://dx.doi.org/10.1038/nature09882.

Willer G.B., Lee V.M., Gregg R.G., Link B.A., 2005. **Analysis of the Zebrafish perplexed mutation reveals tissue-specific roles for de novo pyrimidine synthesis during development.** Genetics, 170(4):1827-37. https://doi.org/10.1534/genetics.105.041608.

Wittkopp N., Huntzinger E., Weiler C., Saulière J., Schmidt S., Sonawane M., Izaurralde E., 2009. **Nonsense-mediated mRNA decay effectors are essential for zebrafish embryonic development and survival.** Mol Cell Biol., 29(13):3517-28. https://doi.org/10.1128/MCB.00177-09.

Xue F., Zhang H., 2017. **Signaling pathway of mitochondrial stress.** Frontiers in Laboratory Medicine,1:40-42. https://doi.org/10.1016/j.flm.2017.02.009.

Zhang C., Chu M., 2018. Leflunomide: **A promising drug with good antitumor potential.** Biochem Biophys Res Commun, 496(2):726-730. https://doi.org/10.1016/j.bbrc.2018.01.107.

Zhu, X., Xu Y., Yu S., Lu L., Ding M., Cheng J., Song G., Gao X., Yao L., Fan D., Meng S., Zhang X., Hu S., Tian Y., 2014. **An efficient genotyping method for genome-modified animals and human cells generated with CRISPR/Cas9 system.** Sci Rep, 4:6420. http://dx.doi.org/10.1038%2Fsrep06420.

Acknowledgements

Circa quattro anni fa ho intrapreso il mio percorso all'Università di Padova, che non avrebbe avuto inizio senza la fiducia che il prof. Argenton ha riposto in me. In questi anni è stato per me più che un tutor, un mentore. Aperto al confronto e sempre disponibile all'ascolto, ha affidato nelle mie mani un progetto ambizioso su una proteina che è oggetto di studio da decenni. Mi ha sostenuta aiutandomi a superare ostacoli, spronandomi, e facendo crescere in me autonomia, intraprendenza, senso critico e di responsabilità. Qualunque frase di ringraziamento non potrebbe descrivere adeguatamente la mia gratitudine nei Suoi confronti. Non esiste "un'altra alternativa".

Se potessi paragonare i tre anni di dottorato ad un viaggio, senza dubbio la mia compagna di viaggio è stata Margherita. Con il suo raro altruismo, senso del dovere e valore professionale oltre che personale, ha rappresentato per me un esempio e, soprattutto, una sorella. Abbiamo condiviso clonaggi, voli intercontinentali, ansie e gioie, banconi e pipette, ma soprattutto abbracci e sorrisi. Non potrei mai rivivere gli anni trascorsi senza pensare a lei e ringraziarla.

Il laboratorio è stato la mia seconda casa, e come in ogni casa che si rispetti non posso non menzionare il resto della famiglia. In particolare, voglio ringraziare la prof.ssa Tiso, Nicola, Stefania, Giacomo, Marco, Elisa, Claudio e Alberto, sia per il loro supporto professionale che per la loro amicizia.

Infine, ogni dottorato che si rispetti è fatto di alti e bassi, risultati e sconfitte, sacrifici e soddisfazioni. Il più grande sacrificio è stata la lontananza da voi, punti fermi nella mia vita e miei primi sostenitori. È a voi che devo tutto quello che sono e che sarò.